國立交通大學

電子工程學系 電子研究所碩士班

碩 士 論 文

TFT 液晶顯示面板的 Mura 瑕疵自動偵測

Automatic Mura Defect Detection on

TFT Liquid Crystal Display Panels

指導教授：王聖智　博士

研 究 生：方立德

中 華 民 國 九 十 四 年 九 月

TFT 液晶顯示面板的 Mura 瑕疵自動偵測

Automatic Mura Defect Detection on TFT Liquid Crystal Display Panels

研 究 生: 方立德　　　　　　Student: Li-Te Fang

指導教授: 王聖智　　　　　　Advisor: Sheng-Jyh Wang

國 立 交 通 大 學

電子工程學系電子研究所碩士班

碩 士 論 文

A Thesis
Submitted to the Institute of Electronics
College of Electrical Engineering and Computer Science
National Chiao Tung University
in Partial Fulfillment of Requirements
for the Degree of
Master of Science
in
Electronics Engineering
September 2005
Hsinchu, Taiwan, Republic of China

中華民國九十四年九月

授權書

(博碩士論文)

本授權書所授權之論文為本人在_____大學(學院)_____系所_____組_____學年度第_____學期取得_____士學位之論文。

論文名稱：_____

1.□同意　　　□不同意

本人具有著作財產權之論文全文資料，授予行政院國家科學委員會科學技術資料中心、國家圖書館及本人畢業學校圖書館，得不限地域、時間與次數以微縮、光碟或數位化等各種方式重製後散布發行或上載網路。

本論文為本人向經濟部智慧財產局申請專利的附件之一，請將全文資料延後兩年後再公開。(請註明文號:　　　　　　　　　　　　　　　　)

2.□同意　　　□不同意

上述授權內容均無須訂立讓與及授權契約書。依本授權之發行權為非專屬性發行權利。依本授權所為之收錄、重製、發行及學術研發利用均為無償。上述同意與不同意之欄位若未鉤選，本人同意視同授權。

指導教授姓名：

研究生簽名：　　　　　　　　　　　　　　學號：

（親筆正楷）　　　　　　　　　　　　　　（務必填寫）

日期：民國　　　年　　　月　　　日

1. 本授權書請以黑筆撰寫並影印裝訂於書名頁之次頁。

2. 授權第一項者，所繳的論文本將由註冊組彙總寄交國科會科學技術資料中心。

3. 本授權書已於民國 85 年 4 月 10 日送請內政部著作權委員會（現為經濟部智慧財產局）修正定稿。

4. 本案依據教育部國家圖書館 85.4.19 台(85)圖編字第 712 號函辦理。

國立交通大學

論文口試委員會審定書

本校＿＿＿＿＿＿＿＿＿＿碩士班＿＿＿＿＿＿＿＿＿＿君
所提論文＿＿＿＿＿＿＿＿＿＿＿＿＿＿＿＿＿＿＿＿＿
合於碩士資格水準，業經本委員會評審認可。

口 試 委 員：

＿＿＿＿＿＿＿＿＿＿　　　＿＿＿＿＿＿＿＿＿＿
王　聖　智　　　　　吳　文　榕

＿＿＿＿＿＿＿＿＿＿　　　＿＿＿＿＿＿＿＿＿＿
辛　正　和　　　　　黃　仲　陵

指 導 教 授：

＿＿＿＿＿＿＿＿＿＿
王　聖　智

所　　　長：

＿＿＿＿＿＿＿＿＿＿
陳　紹　基

系 主 任：

＿＿＿＿＿＿＿＿＿＿
李　鎮　宜

中華民國九十四年 七 月 二十九 日

TFT 液晶顯示面板的 Mura 瑕疵自動偵測

研究生: 方立德　　　　　　　　　　　指導教授: 王聖智 博士

國立交通大學

電子工程學系 電子研究所碩士班

摘要

在本文中，我們提出一個能夠自動偵測 LCD 面板上四種不均勻(Mura)瑕疵型態的演算法。這四種瑕疵是分別是群聚型瑕疵、垂直塊狀瑕疵、刮痕狀瑕疵、以及漏光瑕疵。要偵測群聚型瑕疵，我們使用了 Laplacian of Gaussian (LOG)濾波器。要偵測垂直塊狀型瑕疵，我們檢查原始影像一維投影的曲率變動。要偵測刮痕狀瑕疵，我們設計了一個頻率域上的濾波器來偵測特定的頻率成分。要偵測漏光瑕疵則是利用影像鏡面的方式並且採用偵測與群聚狀瑕疵相同的 LOG 濾波器方法。這四種不均勻的瑕疵偵測方式被整合成一個有效系統。實驗的結果證明這些演算法的確可以很有效率地偵測出 LCD 面板上的這四種 Mura 瑕疵。

Automatic Mura Defect Detection on TFT Liquid Crystal Display Panels

Student: Li-Te Fang   Advisor: Dr. Sheng-Jyh Wang

Institute of Electronics
National Chiao Tung University

Abstract

In this thesis, we propose an automatic inspection system, which can automatically detect four types of Muras on an LCD panel: Cluster Mural, V-band Mura, Rubbing Mura, and Light Leak Mura. To detect cluster Mura, the Laplacian of Gaussian (LOG) filter is used. To detect v-band Mura, we check the variation tendency of the projected 1-D intensity profile. To detect rubbing Mura, we designed a frequency mask to detect distinct components in the frequency domain. To detect light leak Mura, we apply image mirroring and adopt the same LOG filter used in detecting cluster Muras. All four types of Mura detection are integrated together into an efficient system. Simulation results demonstrate that the proposed automatic Mura detection algorithms can efficiently detect these four types of mura defects on LCD panels.

誌謝

特別感謝我的指導教授 王聖智老師，除了對我們在研究上悉心的教導與激勵，讓我們持續的努力不懈，還有處處為學生著想，讓我們有個良好的研究環境，不會有後顧之憂。感謝實驗室的全體夥伴們，特別是昭穎，紹宇，世軒，文翰，因為你們的鼓勵生活上的協助以及學業上的討論，這篇論文才得以順利的完成。特別是感謝博士班學長信嘉，在你的幫助下讓我逐漸的學習成長，才能順利的進行研究。最後要感謝我的家人，因為他們的鼓勵，我才能在困難之中持續的努力。

Index

LIST OF FIGURES

List of Tables

Chapter 1　Introduction

As TFT-LCD (Thin Film Transistor Liquid Crystal Display) devices get more and more popular in display market, the inspection of LCD quality has been receiving increasing attention. So far, most inspection methods depend on the perception of human eyes. However, there are many disadvantages in human inspection: high labor power, inconsistent detection, and limitations in visual sensitivity. Hence, automatic inspection based on machine vision could be another option for the inspection of LCD panels.

In this thesis, we propose an automatic inspection system for the inspection of visual defects on TFT-LCD panels. These visual defects are usually called muras in the literature. They are defined as visible imperfections on an active LCD display screen. A typical mura usually appears as a low-contrast and non-uniform region and is typically larger than a single pixel [1]. The causes of muras are due to the imperfection manufactures of various components or foreign particles within the liquid crystal. Several efforts have already been spent to classify these defects and to establish the evaluation standards [1-2]. Several detection algorithms, on the other hand, have also been proposed in the literature [3-8].

In this thesis, we focus on the detection of four types of Muras. The contents of this thesis are organized as follows. In Chapter 2, we introduce the background of LCD components, human vision system, related researches and existing Mura detection algorithms. In Chapter 3, we describe the inspection procedure of our Mura inspection system and present several Mura detection algorithms. Experiments are then presented in Chapter 4. Finally, in Chapter 5, we conclude our work.

Chapter 2 Background

In this chapter, we'll first introduce major LCD components and the causes of Mura defects. Then we will discuss the capability of human vision perception in terms of just noticeable difference (JND). Since some associations have already standardized Mura defects, we will introduce the defined Mura types and the evaluation formulae of Mura in these standards. Finally, we will give an overview of existing Mura detection algorithms.

2.1 LCD components

In this thesis, we focus on the development of detection algorithms for the inspection of the FOS (Front Of Screen) quality of an active matrix thin-film transistor liquid crystal display (AM TFT-LCD). Figure 2-1 illustrates the cross-section of an AM TFT-LCD. According to Y. Mori's classification, various causes, as listed in Table 2-1, could produce defects. Basically, an LCD display includes two essential components: 1) Cell Unit and 2) Backlight Unit. In the cell unit, there are five elements: (1) liquid crystal, (2) thin-film-transistor (TFT) array, (3) color filters, (4) glasses and (5) polarizer. In general, the functionality of cell unit is to make the RGB color switching at each pixel controllable. On the other hand, in the backlight unit, there are four basic elements: (1) lamp, (2) light pipe, (3) reflective film and (4) optical film. Generally, the functionality of backlight unit is to produce uniform light.
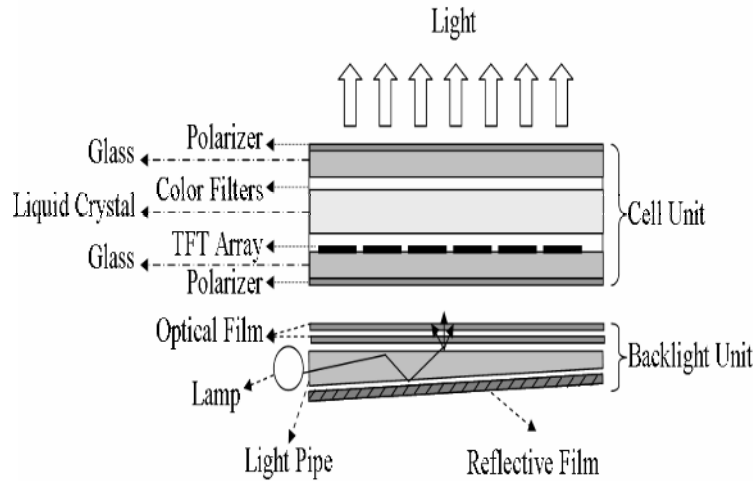
Figure 2-1 Cross-section of an active matrix TFT-LCD

2.1.1 Causes of Mura for TFT-LCD

In the inspection of FOS quality, the so-called Mura defects greatly influence the FOS quality [1]. Mura defects are defined as these visible imperfections of the FOS image of a display screen in active use. In [3], Mori et al listed several causes of Mura defects in TFT-LCD, as shown in Table 2-1. Usually, the manufacturing performance of every component in the cell unit or the backlight unit will affect the appearance of Mura defects. A superior manufacture process will cause less Mura defects, while an inferior manufacture process will induce more visible Mura defects. Usually, the non-uniformity in various kinds of components induces different kinds of Mura defects.

The Non-uniform gap between glasses will induce Cluster Muras while the non-uniformity of color filter usually causes color Muras. Wrinkled optical filters usually induce Light Leak Muras, and non-uniform lamp's rays usually cause gradation Muras. On the other hand, a so-called "rubbing" process is usually used to achieve LCD alignment by reordering liquid crystal cell along a certain direction. This 'Rubbing process' may causes Rubbing Muras.

3

Table 2-1 Causes of Mura defects for TFT-LCD [3]

Basic Unit	Causes of Mura
Cell unit	(1) Non-uniform gap between glasses
	(2) Non-uniform color of color filter
	(3) Non-uniform density of liquid crystal
	(4) Non-uniform thickness of TFT array layer
Backlight unit	(5) Wrinkled optical filter
	(6) Non-uniform lamp's rays
	(7) Warped light pipe

2.1.2 Introduction of Mura Types

Mura is a non-uniform brightness region in the FOS image of an LCD. There are several existing Mura types, such as Cluster Mura, Gradation Mura, line Mura, region Mura,.and so on. We will show some of the Mura type in the following figures.

(a)   (b)
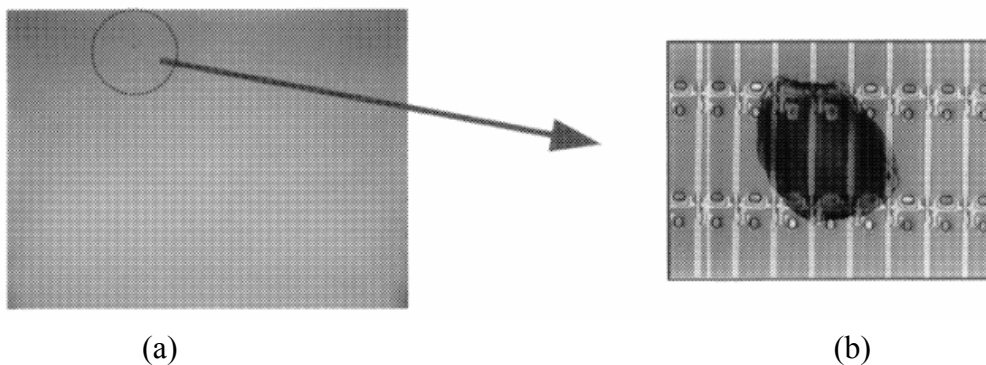
Figure 2-2 (a) A Cluster Mura and (b) microscope image of a contamination on the TFT

array that causes a Cluster Mura. [4]

| (a) | (b) |
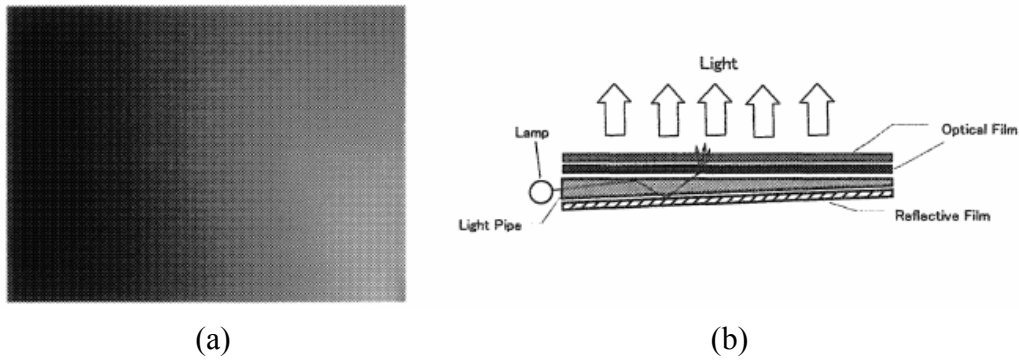
Figure 2-3 (a) A Gradation Mura (b) cross-sectional schematic illustration of backlight [4]
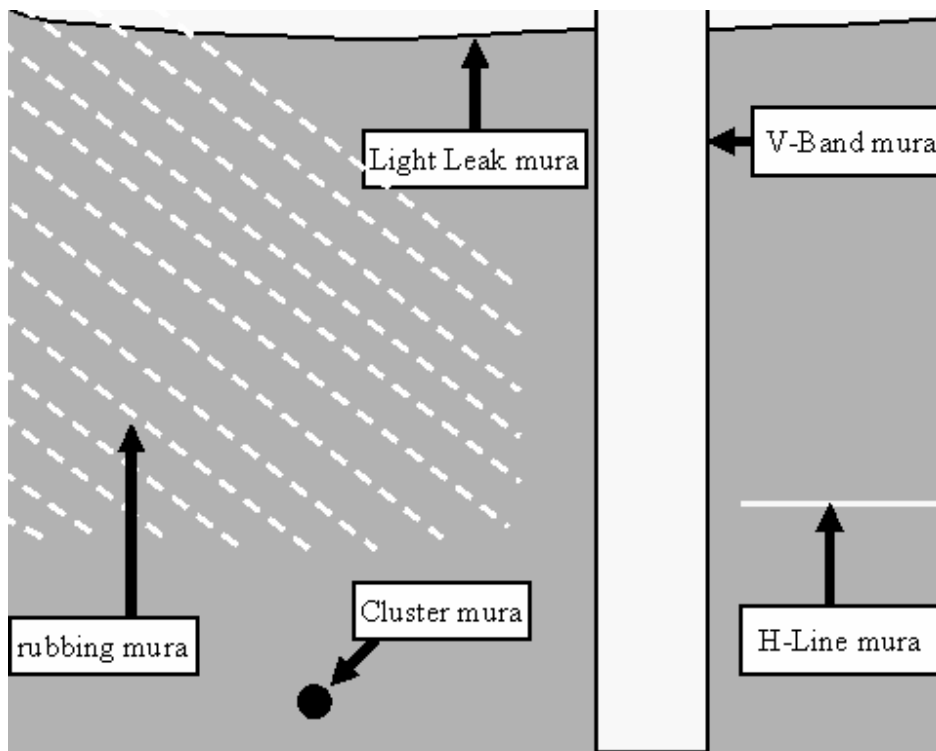
Figure 2-4 Example of Mura types on TTLA LCD

Figure 2-2 shows an example of Cluster Mura, which is a small dark spot caused by non-uniformity of the cell, non-uniformity of color filters, contaminations in the cell, and so on. Figure 2-3 (a) shows luminance gradients where the right region of the screen is brighter than the left region. It seems this defect is caused by non-uniformity of the backlight and is called a "Gradation Mura". Figure 2-3 (b) shows the cross-sectional illustration of the backlight. The backlight consists of various components. In the backlight unit, non-uniform lamp's ray, wrinkled optical film, and

warped light pipe tend to cause Gradation Muras [4]. Finally, in Figure 2-4, we show some examples of s Mura defects on TTLA LCD. These are the major types of muras that we want to detect.

2.2 Human visual contrast and just noticeable distortion

Traditionally, mura defects on LCD panels are to be inspected by human eyes. If we want to inspect mura defects with machine vision, we need to define some objective measures that are closely related to human's subjective visual perception about the degree of mura defects. In [2], it has been indicated that the minimum perceivable contrasts of a defect is closely related to its size and shape. Based on this phenomenon, a so-called Semu value is defined to measure the degree of mura defects [2]. In this section, we will especially discuss the sensitivity of human visual contrast and just noticeable distortion (JND).

2.2.1 Contrast Sensitivity

Human visual perception is sensitive to the contrast of luminance. Till now, three types of contrast definitions have been widely used in the world.

For a periodic pattern of symmetrical deviations, ranging from Lmin to Lmax, Michelson contrast is defined as

$$C_M = \frac{L_{max} - L_{min}}{L_{max} + L_{min}}.$$ (1)

When the pattern is an increment or a decrement of ΔL with respect to a uniform background with luminance L, Weber's contrast is defined as

$$C_W = \frac{\Delta L}{L}$$ (2)

To measure the contrast sensitivity of complex images, the above two definitions are usually not sufficient enough. For example, if (1) or (2) is adopted to define contrast, the appearance of a very bright or a very dark point in the image will seriously affect the measure of image contrast. Moreover, it is the local luminance average, instead of the global luminance average, that influences human perception about image contrast Hence, to define contrast for complex images, Peli proposed a local band limited contrast measure in [14]. His definition about contrast is expressed as

$$Ci(x, y) = \frac{BP_i(x, y)}{LP_i(x, y)}$$ (3)

where $BP_i(x,y)$ is the bandpass image of the ith band at location (x, y), and $LP_i(x,y)$ contains the energy of all the subbands below the ith band at location (x, y). Several different modifications of this contrast definition have been used to measure contrast sensitivity. In [13], some psychophysical experiments had demonstrated good agreement with Peli's definition based on Gabor patches.

Contrast sensitivity can be described as a function of spatial frequency. This function is called contrast sensitivity function (CSF). Contrast sensitivity is defined as the inverse of contrast threshold, which is the minimum contrast necessary for an observer to detect the targets.

In [16], Mannos and Sakrison first applied an HVS (Human Visual System) model to image coding. They modeled the HVS as a nonlinear point transform followed by the modulation transform function (MTF) of the form:

$$H(f) = 2.6(0.192 + 0.114f)\exp(-(0.114f)^{1.1})$$ (4)

In [17], Nill proposed a new function of MTF that can be used for DCT (Discrete Cosine Transform) transform

$$H(f) = (0.2 + 0.45f)\exp(-0.18f) \quad (5)$$

In [18], Ngan et al proposed another definition of MTF, which is expressed as

$$H(f) = (0.31 + 0.69f)\exp(-0.29f) \quad (6)$$

In spite of the dependence on spatial frequency, the contrast sensitivity also depends on temporal frequency. Therefore, the contrast sensitivity can be described as the combinational function of spatial frequency and temporal frequency. In [19], Kelly proposed a contrast sensitivity function based on spatial and temporal frequency and the function is formulated as

$$CSF(f_s, f_t) = 4\pi^2 f_s f_t \exp(\frac{-4\pi(f_t + 2f_s)}{45.9}) \times (6.1 + 7.3 \left| \log(\frac{f_t}{3f_s}) \right|^3) \quad (7)$$

This CSF function reflects that human eyes have lower sensitivity at low and high spatial (temporal) frequency and higher sensitivity at medium spatial (temporal) frequency.
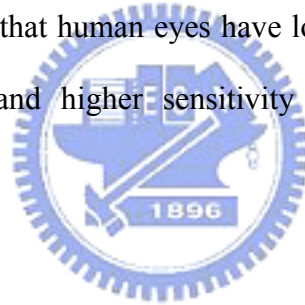
2.2.2 Just-Noticeable Distortion

The definition of just-noticeable distortion (JND) is the visibility threshold of distortion, below which the reconstruction errors are imperceptible [20]. As mentioned above, human eyes are more sensitive to luminance contrast than to absolute luminance value. Furthermore, the average value of background luminance will influence the sensitivity of human visual perception. In Weber's law, the ratio of just noticeable luminance difference to stimulus' luminance is almost constant. From the viewpoint of JND, we just need to detect these defects whose contrast is above this threshold.

In [21], the JND profile of a still image is represented as a function of local signal properties, such as background luminance, activity of luminance changes and dominant

spatial frequency. Here, JND is defined as

$$JND_S(x, y) = \max\{f_1(mg(x, y)), f_2(bg(x, y))\}, 0 \le x < H, 0 \le y < W \quad , \tag{8}$$

where H and W denote the horizontal and vertical dimensions of the still image. f1 represents the error visibility threshold due to texture masking and f2 represents the error visibility threshold due to average background luminance. mg(x, y) denotes the maximal weighted average of luminance gradients around the pixel at location (x, y) and bg(x, y) is the average background luminance around the pixel at location (x, y).

In [22], mg(x, y) of the pixel at (x, y) is determined by calculating the weighted average of luminance changes around the pixel in four directions, expressed as

$$mg(x, y) = \max_{k=1,2,3,4}\{|grad_k(x, y)|\} \tag{9}$$

and

$$grad_k(x, y) = \frac{1}{16}\sum_{i=1}^{5}\sum_{j=1}^{5} p(x-3+i, y-3+j) \cdot G_k(x, y), 0 \le x < H, 0 \le y < W \tag{10}$$

where p(x, y) denotes the pixel at (x, y). These four operations, Gk(i, j) for k = 1,2,3,4 and i, j = 1,2,3,4,5, are shown in Figure 2-5.
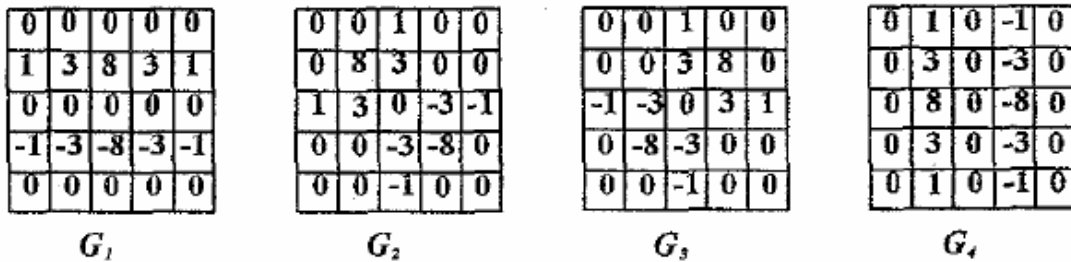
Figure 2-5 Operators for the calculation of the weighted average of luminance changes along four directions. [20]

The value of f1(mg(x, y)) is calculated as

$$f_1(mg(x, y)) = mg(x, y) \times \beta, 0 \le x < H, 0 \le y < W \quad , \tag{11}$$

where the value of β is gotten from a subject test and its value is chosen to be 2/17. bg(x,

9

y) is calculated based on a weighted low-pass operator, B(i, j), i, j = 1,2,3,4,5, and is expressed as

$$bg(x, y) = \frac{1}{32} \sum_{i=1}^{5} \sum_{j=1}^{5} p(x-3+i, y-3+j) \cdot B(i, j), 0 \le x < H, 0 \le y < W \qquad (12)$$

B

Figure 2-6 The operator for the calculation of average background luminance.

[20]

The relationship of between visibility threshold and the average background bg(x, y) is shown in Figure 2-7
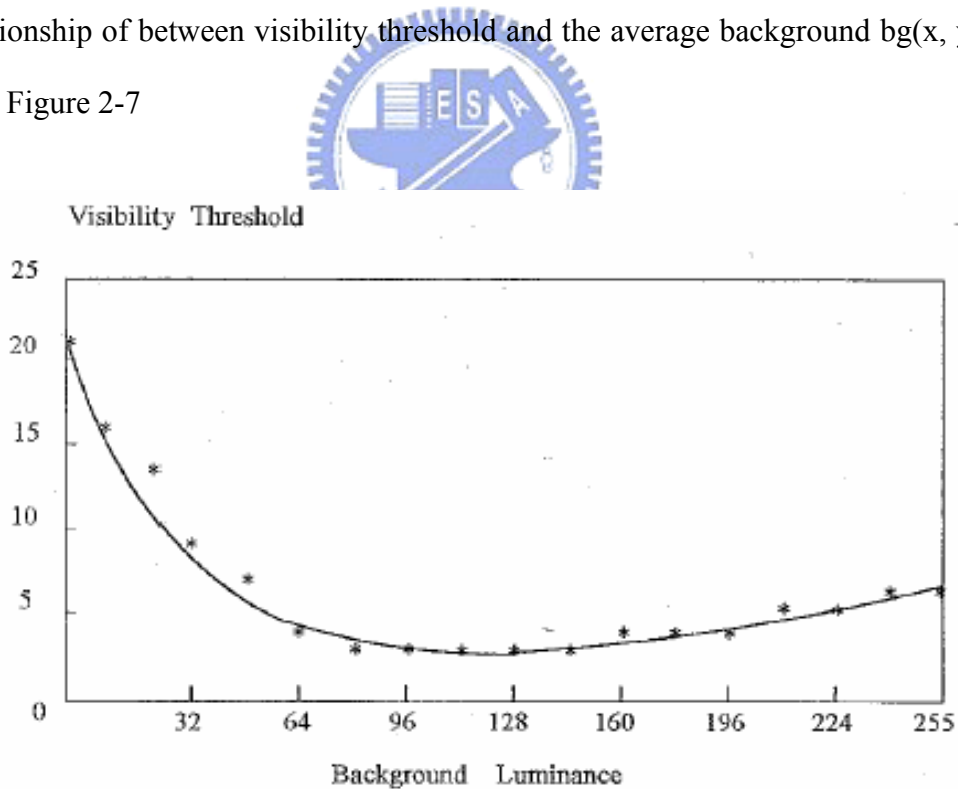
Figure 2-7 Error visibility thresholds due to background luminance in the

spatial domain [21].

JND can also be calculated on the spatial-temporal domain. The process to get this value is to multiply spatial JND and temporal JND, as expressed below [21]:

$$JND_{S-T}(x, y, n) = f_3(ild(x, y, n)) \cdot JND_S(x, y, n) \qquad (13)$$

where ild(x, y, n) is the average interframe luminance difference between the nth and

(n-1)th frame at pixel (x, y):

$$ild(x, y, n) = \frac{p(x, y, n) - p(x, y, n-1) + bg(x, y, n) - bg(x, y, n-1)}{2} \qquad (14)$$

The empirical results of f3 for all possible interframe luminance difference are

shown in Figure 2-8.
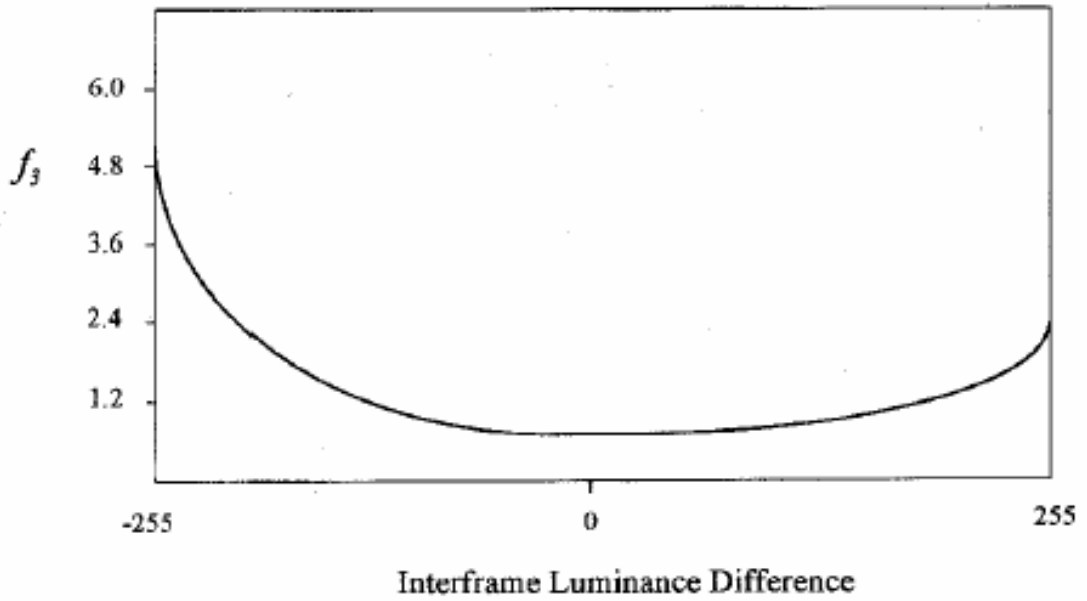
Figure 2-8 Error visibility threshold in the spatial-temporal domain, which is

modeled as a scale factor of interframe luminance difference and

the JND value in the spatial domain [21]

The error visibility threshold increases when interframe luminance difference

increases. The sensitivity of human vision decreases if the scene changes or there is a

large temporal luminance difference.

2.3 Definition, evaluation and discrimination of Mura on LCD

Recently, several efforts have been spent on the classification of defects and standardization of quality evaluation. For example, the Video Electronics Standards Association (VESA) has standardized the classification of mura defects [1], while the Semiconductor Equipment and Materials International (SEMI) has standardized the defect quantification [2]. Based on properties of human perception, other researches have further improved the analysis methods and proposed several detection algorithms [3-8].

2.3.1 Definition of Mura in VESA

The FPDM2 (Flat Panel Display Measurements，Version 2.0) standard of VESA (Video Electronics Standards Association) defines Muras to be low contrast, non-uniform brightness regions, typically larger than a single pixel. The captured DUT(Display under test) image is processed by MuraTool according to Photon Dynamics Inc. This Mura Tool is capable of detecting multiple classes of defects, as specified in Table 2-2.

In the 15 phases defined by VESA, Phases 1~5 are more obvious defects, Phase 6~11 are less obvious defects, and Phases 12~15 are block or non-uniform defects. Additional Mura defect classes can be defined in the future version of this specification. Figure 2-9 shows some examples of Mura types.

(a) S-line, G-line, black and white Spot, bright border bloom and fill port defect

(b) Rubbing line defect

(c) Bright and dark region defect

(d) Block defect
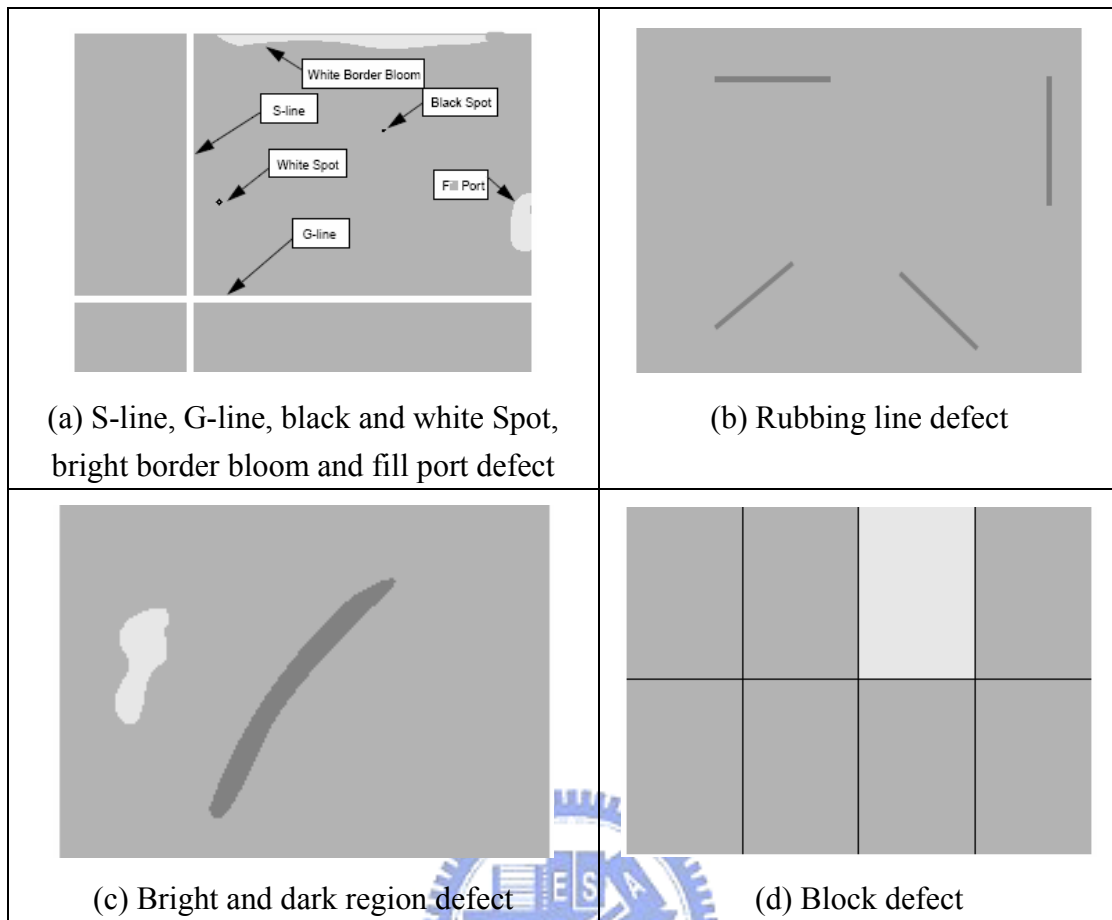
Figure 2-9 Example of Mura types in VESA

Different Muras have different features. Hence, a Mura detection system usually adopts several detection algorithms at the same time. In MuraTool, it uses morphological methods to segment and classify Muras, as shown in Figure 2-10. In the initialization step of the algorithm, edges of the DUT are detected first, and an active region rectangular display $L(x,y)$ is passed to the Segmentation step of the algorithm. The segmentation component sequentially examines the DUT image to perform 15 phases of detection. At each phase, a Boolean blob is generated if any potential defect is detected. The blob mask is in the TRUE state wherever a potential defect exists, and is in the FALSE state otherwise. Figure 2-11 illustrates a blob mask with a single blob.

Table 2-2 Defect detection phases and defect classes in FPDM2 [1]

Phase	Class	Class description	Examples of physical LCD defect types
1	1	column line	signal line
2	2	row line	gate line
3	3	random thin line pattern	straw pattern, irregular thin dark streaks
4	4-1	white interior spot	bright pixel, bright pixel cluster, bright spot
4	4-2	white corner bloom	bright corner
4	4-3	white border bloom	bright panel edge
5	5-1	black interior spot	dark pixel, dark pixel cluster, dark spot
5	5-2	black corner bloom	dark corner
5	5-3	black border bloom	dark panel edge
6	6	thin horizontal line	thin rubbing line
7	7	thin vertical line	thin rubbing line
8	8	thin positive slope diagonal line	thin rubbing line
9	9	thin negative slope diagonal line	thin rubbing line
10	10-1	bright region	elliptical region, wide rubbing line, bright streak, bright arc
10	10-2	bright region collection	bright ring, bright streaks, bright arcs
11	11-1	dark region	elliptical region, wide rubbing line, dark streak, dark arc
11	11-2	dark region collection	Newton ring, vertical periodic lines, dark streaks, dark arcs
12	12	wide horizontal line	panel driver block, lithography mis-alignment
13	13	wide vertical line	panel driver block, lithography mis-alignment
14	14-1	bright region non-uniformity	brightness non-uniformity of panel or backlight
14	14-2	bright border non-uniformity	fill port
15	15-1	dark region non-uniformity	darkness non-uniformity of panel or backlight
15	15-2	dark border non-uniformity	fill port
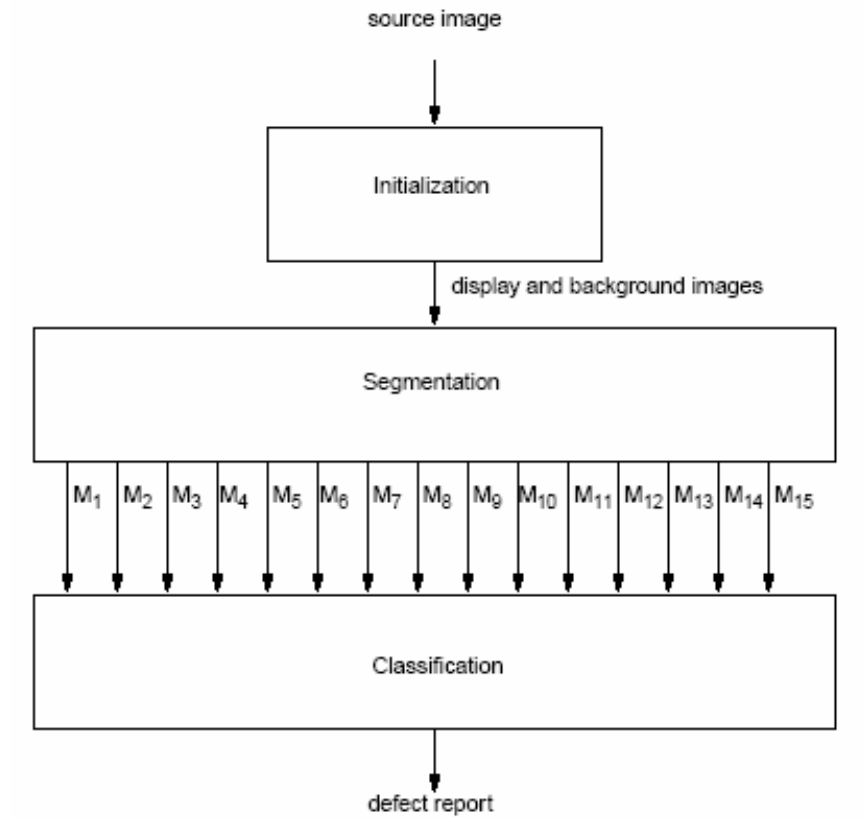
Figure 2-10 Flowchart of MuraTool [1]
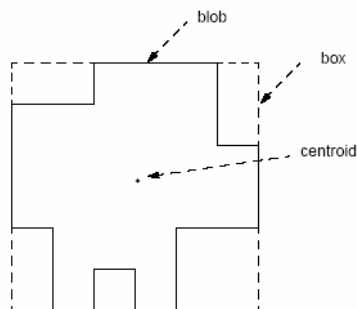
Figure 2-11 A blob and its boundary box

In the classification step, the image data masked by each blob mask are examined. If the average or peaks contrast of the detected region is above a contrast threshold, that region is classified as a defect. The contrast threshold can be manually set. In [1], the average contrast is defined as

15

$$C_A = \frac{\sum_x \sum_y |L(x, y) - B(x, y)|}{\sum_x \sum_y B(x, y)} \tag{15}$$

where L(x,y) represents pixel amplitude in the defect region and B(x,y) represents the pixel amplitude in the background. The peak contrast is defined as

$$C_P = \frac{MAX\limits_{x,y} (|L(x, y) - B(x, y)|)}{B(x_m, y_m)} \tag{16}$$

.

After all the processes, the MuraTool produces a defects report file, as shown in Table 2-3.

Table 2-3 Example of Mura defect file presented in LCD pixel unit

Filename: Panel.LCDBlobs

Blob	x	y	Width	Height	Area	Type	Contrast	Phase	Class	Result
1	185.90	300.50	5.58	600.50	3048.1	P	80.33	1	1	Defect
2	400.50	300.50	800.50	5.58	4068.3	P	80.33	2	2	Defect
3	77.96	56.43	5.58	5.58	26.3	P	50.24	4	4-1	Defect
4	725.58	543.30	5.58	5.58	26.3	P	10.16	4	4-1	
5	725.58	56.43	5.58	5.58	26.3	P	9.86	5	5-1	
6	77.96	543.30	5.58	5.58	26.3	P	49.97	5	5-1	Defect
7	650.66	78.04	108.44	10.67	1098.2	P	6.13	6	6	Defect
8	650.66	521.69	108.44	10.67	1098.2	P	6.39	6	6	Defect
9	702.72	177.19	11.93	81.86	920.6	P	6.78	7	7	Defect
10	702.72	423.81	11.93	81.86	920.6	P	7.03	7	7	Defect
11	479.23	86.94	67.80	67.87	1090.1	P	4.84	8	8	Defect
12	479.23	370.42	67.80	67.87	1088.5	P	5.08	8	8	Defect
13	479.23	229.31	67.80	67.87	1090.1	P	4.84	9	9	Defect
14	479.23	512.79	67.80	67.87	1088.5	P	5.08	9	9	Defect
15	617.37	441.60	52.56	43.72	1793.9	P	8.68	10	10-1	Defect
16	617.37	158.13	39.87	53.89	1756.8	P	8.68	11	11-1	Defect

2.3.2 Definition of Mura in SEMI

On the other hand, the Semiconductor Equipment and Materials International (SEMI) have spent a lot of efforts on the standardization of defect quantification. The SEMI D31-1102 standard defines Mura in terms of luminance [2].

Based on sensory analysis, quantitative evaluation method of Mura on liquid crystal displays (LCD's) was investigated. They conducted a perception test by using pseudo Mura to figure out the relationship between "just noticeable differences"(JND) and the size of Mura. This approach intends to clarify the detection method and to create an automated Mura inspection process. The quality level of a Mura can be described as a function of area and contrast. Then they provide the evaluation standard 'Semu' to analyze the level of Mura defects.

Experiment

In the experiment, pseudo Muras with different combinations of background and luminance are displayed on the LCD. An observer was asked to observe the pseudo Mura and to control the luminance of the pseudo Mura, as illustrated in Figure 2-12. The experiment results are shown in Figure 2-13.
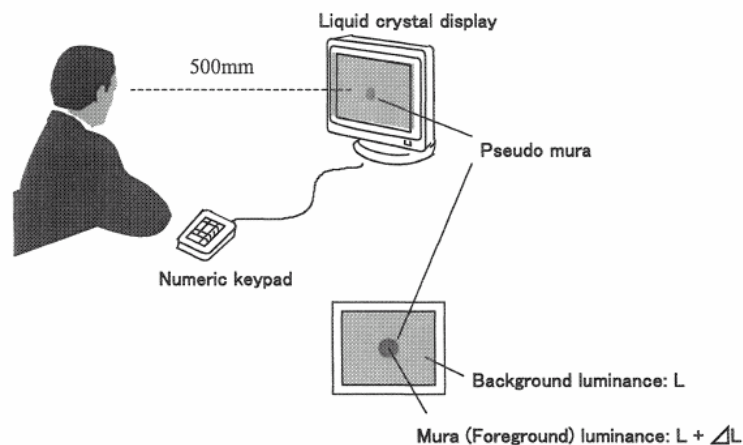
Figure 2-12 Illustration of SEMI Experiment [4]
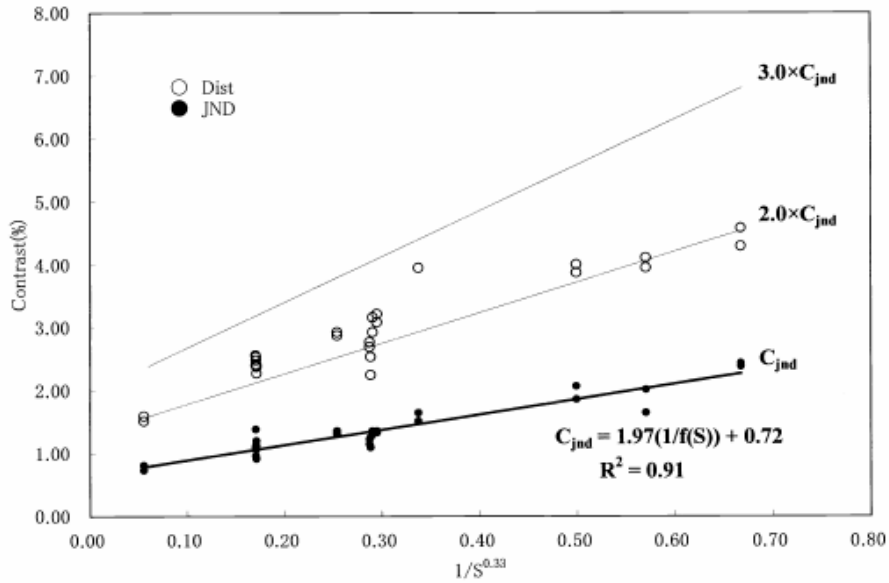
Figure 2-13 Experiment results of SEMI experiment [4]

In the experiment results, several important characteristics were observed:

- The larger the Mura area is, the easier to perceive the Mura. In this case, the Cjnd is smaller.

- The contrast of a pixel Mura must be 1.5~2 stronger to be inspect by human eyes.

- There is no difference between experts and normal people in observing Mura.

- Opposite to experts, the distinct contrast of normal people spreads over a larger range.

SEMI defines the evaluation standard Semu (SEMI Mura) based on Cjnd. The Semu value is formulated as

$$Semu = \frac{|C_x|}{C_{jnd}} = \frac{|C_x|}{(\frac{1.97}{S_x^{0.33}} + 0.72)}$$

(17)

Cjnd : Contrast of the Just Noticeable Difference to human eyes.

Cx : Average contrast of Mura.

18

2.3.3 Further Research on JND Contrast of Mura

In [8], the effect of the background luminance on the Just Noticeable Difference (JND) contrast of Mura was discussed. Three types of Mura, round type, line type, and rectangle type, were under test. The evaluation of JND contrast is tested at 9.8, 41.8 and 97.5 cd/m2. The results showed that there is no significant difference on the JND contrast between 41.8cd/m2 and 97.5 cd/m2. However, the JND contrast at 9.8cd/m2 was higher than that at the other background luminances. The result shows that human perception is more sensitive in the dark background for line type Mura. The following figure shows the evaluation result.
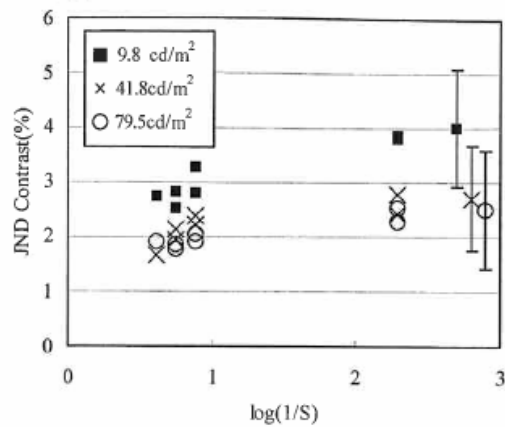
Figure 2-14 The JND contrast of line type Mura [8]
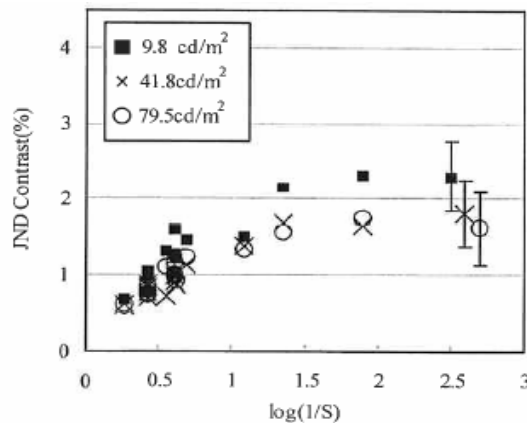
Figure 2-15 The JND contrast of round type and rectangle type [8]

19

Semu formula explains well how Mura strength correlates with the area of Mura (Sx) and the Mura contrast (Cx). However, the sensitivity of human eyes varies under different luminance levels. Hence, a new Semu value is proposed in [8]:

$$\Pr oposed\_Mura\_value = \frac{HVC}{Cjnd\_of\_SEMU} \tag{18}$$

where the JND is calculated as

$$JND\_value_i = 10^{Mura\_transfer_i} \tag{19}$$

with the Mura transfer function being defined as

$$Mura\_transfer_i = a + b \times \log(L_i) + c \times (\log(L_i))^2 \tag{20}$$

Here, a = 1.85832, b = 0.546316, c = -0.0685062.

With the above equations, the HVC is expressed as

$$HVC = JND\_value_j - JND\_value_i \tag{21}$$

(a)   (b)
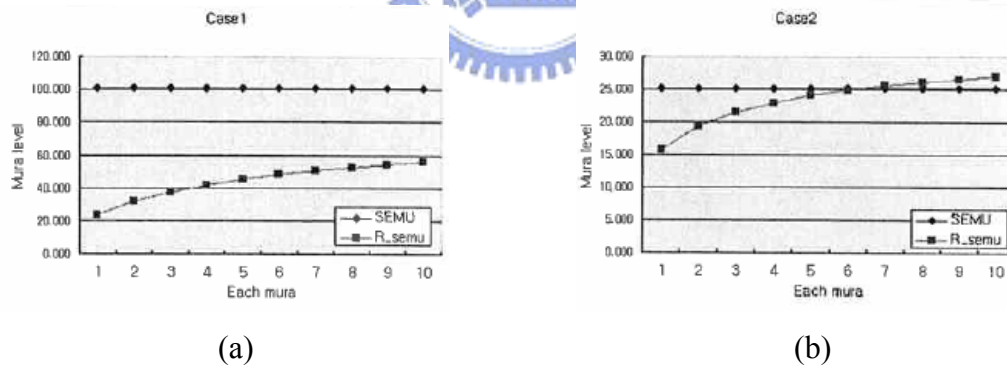
Figure 2-16 Comparison result between Cx and HVC [8]

If the area size is fixed, the human visual contrast (HVC) will change when background varies. However, Cx ratio will be the same in this case. Figure 2-16 shows the Comparison result between Cx and HVC. In this case, Semu will have a same value, for all luminance levels, while the R_semu will change as the HVC changes. As a result, HVC is more suitable than Cx in the evaluation of Mura level.

2.4   Existing Mura detection Methods

Some researches had proposed various methods to detect point and line Muras. In 2004, Jong-Hwan Oh proposed the use of a directional filter bank and adaptive multilevel thresholding to detect Line-defects [10]. On the other hand, Woo-Seob Kim proposed adaptive multilevel thresholding using local block processing methods to detect blob-defects and point-defects [11].

Jae Y. Lee and Suk I. Yoo proposed a modified regression diagnostics and used Niblack's thresholding to detect region-Muras from TFT-LCD panel images [12]. In their approach, the input image of an LCD panel is divided into overlapping windows. Segmentation of region-Mura is performed on each window. Then, the segmentation results of different local regions are merged together into a single image. The merged image is possessed by median filtering, morphological closing, and morphological opening to remove noise. Finally, candidate region-Muras are extracted out and their Mura levels are quantified. The segmentation is completed by using modified regression diagnostics to roughly estimate the background region. Then, subtraction of the background surface from the original window image is used to find a threshold to obtain the binary segmentation result. Figure 2-17 shows the overall inspection procedure. After finding out all candidate region-Muras, they evaluated the Mura levels of all candidate region-Muras. They found that the Mura level claimed by human inspection was greater than 5.5 and they set the Mura level threshold to be 5.5. Figure 2-18 shows the Mura levels of all candidate region-Muras.
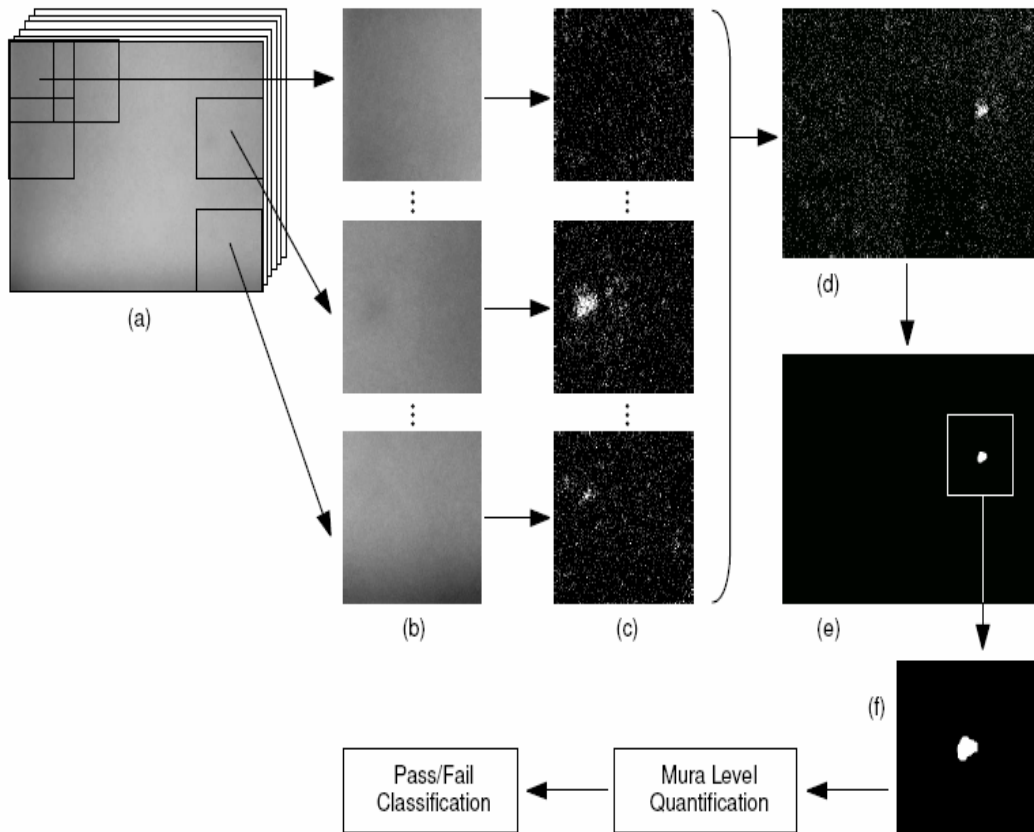
Figure 2-17 Region-Mura inspection procedure in [12] (a) Input image (b) Extracted windows (c) Local segmentation result (d) Merged segmentation result. (e) Post-processed image (f) Extracted candidate region-Mura, whose Mura level is to be quantified
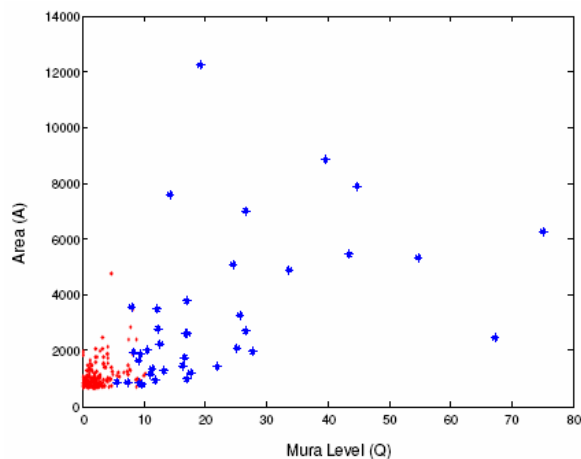
Figure 2-18 Plot of Mura level and area of all candidate region Muras detected in [12]. Candidates claimed by human inspection are denoted by blue asterisk (＊) and the other candidates by red dot (·).

Chapter 3   Automatic Mura detection

algorithms

In this chapter, we will first introduce the setup pf our mura inspection system. Then we'll present a set of automatic inspection algorithms, which can automatically detect four types of Muras on an LCD panel: Cluster Mura, V-band Mura, Rubbing Mura, and Light Leakage Mura. To detect Cluster Muras, the Laplacian of Gaussian (LOG) filter is used. A multi-resolution approach is proposed to detect Cluster Muras of different scales. To speed up the processing speed, this multi-resolution approach is actually implemented in the frequency domain. To detect V-band Muras, we check the variation tendency of the projected 1-D intensity profile. Then, V-band Muras are detected by identifying these portions of the 1-D profile where a large deviation occurs. To detect Rubbing Muras, we designed a frequency mask to detect distinct components in the frequency domain. To detect light leak Muras, we apply image mirroring over the boundary parts and adopt the same LOG filter that has been used in detecting Cluster Muras. All four types of Mura detection are integrated together in an efficient way.

3.1 Inspection Procedure

The inspection system is shown in Figure 3-1. It consists of three major parts: 1) the LCD panel under test, 2) a CCD camera, and 3) a personal computer to execute Mura detection algorithms. The inspection procedure is described as follows. The LCD panel is first placed on the equipment vertically. This panel is driven by a pattern generator to generate patterns of constant gray level. Then, a high-resolution digital

camera takes a few FOS (Front-Of-Screen) images and these FOS images are transmitted to the computer to be inspected by our Mura inspection algorithms. The CCD camera has a 14-bit dynamic range and a spatial resolution of 2048 by 2048 pixels. The detection flow chart of this Mura detection system is illustrated in Figure 3-1 (b).
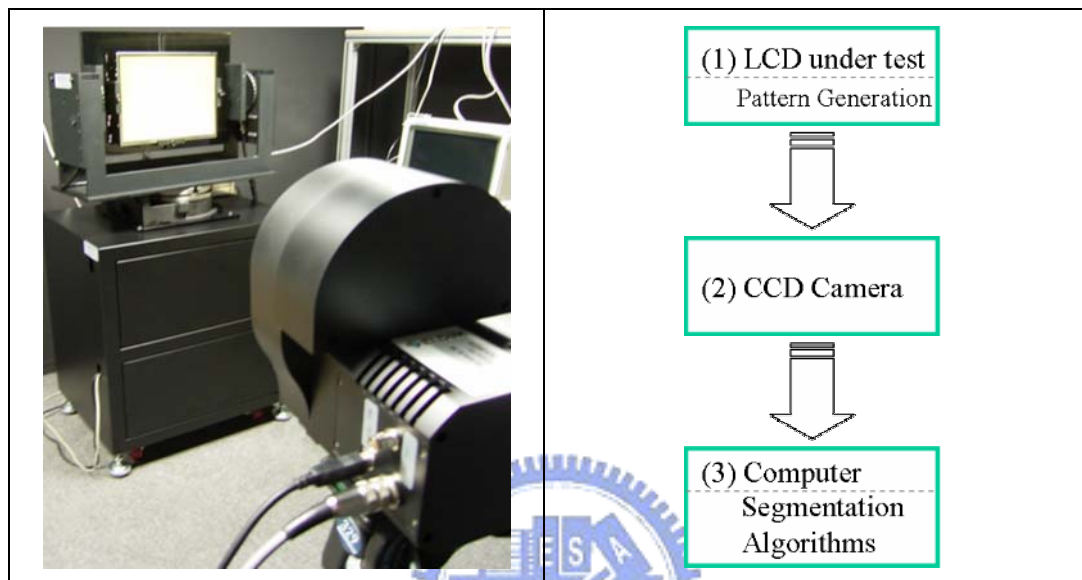
Figure 3-1. (a) Mura inspection system;(b) inspection flowchart.

The inspection system hardware and the driven firmware are set up by TTLA (Taiwan TFT-LCD Association). After the retrieval of the FOS images of LCD panels, we analyze the features of the images and classify the FOS images into different types. According to different features of the image, we extract the Mura defects from the images. The thresholds of our algorithms are selected based on some experiments of human vision test. At the end, the detection result is compared with the original image to ensure to detection result is reasonable. Figure 3-2 shows the block diagram of our automatic Mura detection algorithms.

```
image-retrieving          image-retrieving          TTLA
environment hardware  →   driven software
                      ←
                              ↓
Human vision          ←   Mura image collection  ──────────┐
characteristic simulation  and analysis                    │
      │                           ↓                         │
      │                    Mura image extraction            │
      │                         module                      │
      ↓                           ↓                         ↓
Human vision          ←   Mura image detection  →   detection
model threshold       →        module                result verification
```
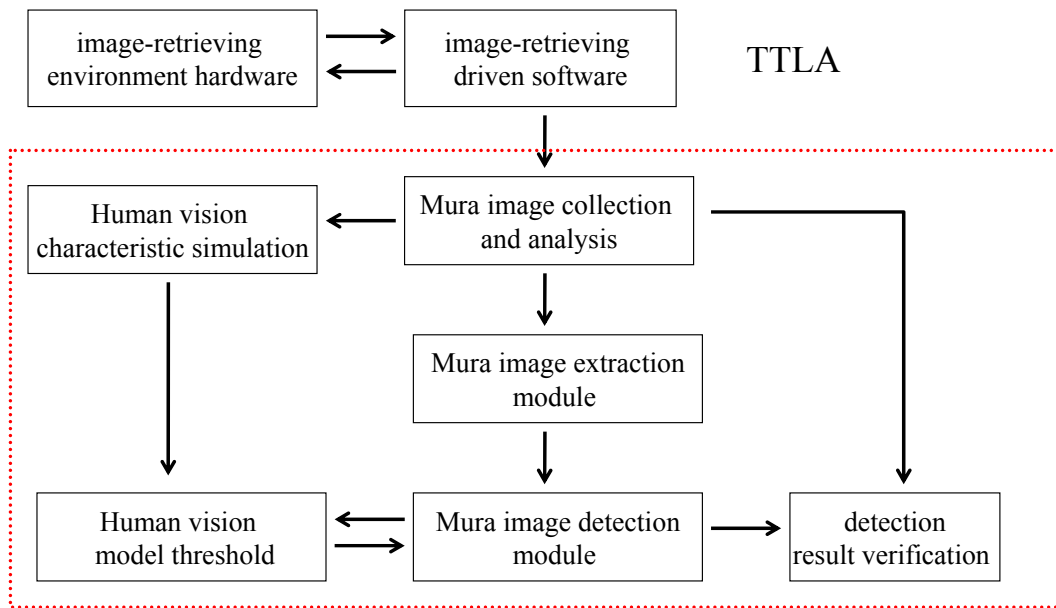
Figure 3-2 Automatic Mura detection algorithms

(a)

(b)

(c)

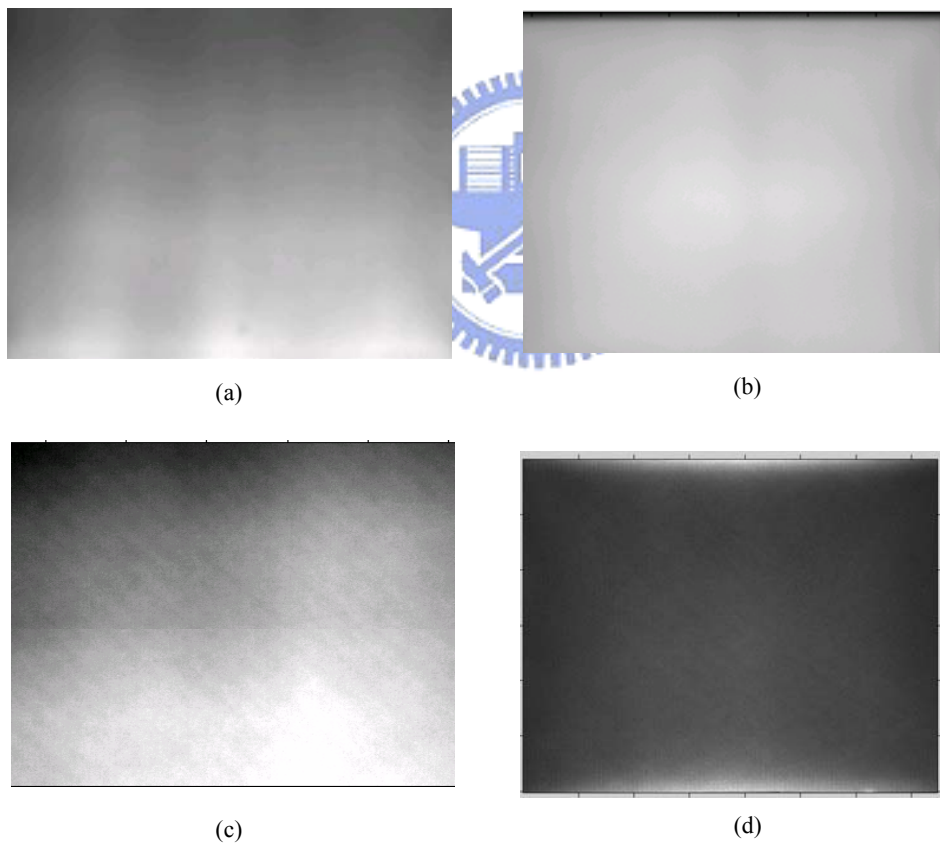(d)

Figure 3-3 (a) Cluster Mura; (b) Vertical Band Mura; (c) Rubbing Mura; (d) Light Leak

Mura.

Among various kinds of Mura defects, our Mura inspection system focuses on the detection of four typical types of Mura defects: Cluster Mura, vertical-band Mura (V-band Mura), Rubbing Mura, and light leak Mura (LL Mura). A Cluster Mura usually appears as a Cluster of dark or bright points in a localized area, as shown at the central bottom of Figure 3-3(a); V-band Mura appears as a wide, vertical stripe with different brightness with respect to the background, as shown in the middle of Figure 3-3(b); Rubbing Mura usually appears as tiled lines with a 45-degree angle spreading over a large region, as shown in Figure 3-3(c); and light leak Mura appears at the boundary of LCD panels, as shown on the top and bottom of Figure 3-3(d).

The inspection procedure of our system is illustrated in Figure 3-4. The LCD panel is first driven by patterns of constant gray level. The image is transmitted to the computer to be processed by the detection algorithms. The detection procedure consists of two major tracks. In one track, the boundary of the FOS image is first padded with mirror images that are to be used for the detection of light-leak Muras. The image is then transformed into the frequency domain to detect Cluster Muras, Rubbing Muras, and light-leak Muras. In the other track, V-band Muras are to be detected in the spatial domain via a curve fitting method. The results of all these four Mura detection algorithms are then combined together to generate the final detection report.
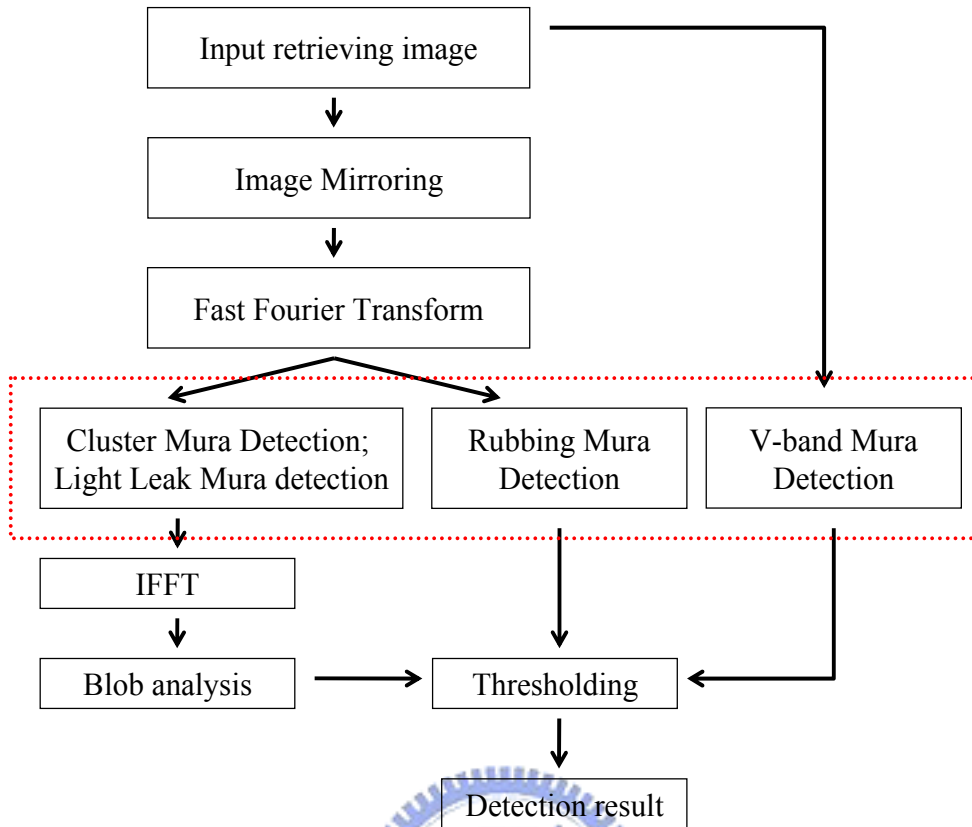
Figure 3-4 Flowchart of Mura detection algorithms

3.2 Inspection of Cluster Mura

Cluster Mura usually appears as a cluster of bright or dark points in a localized area [13]. Generally speaking, there are two types of Cluster Mura: round-type Cluster Mura and line-type Cluster Mura, as shown in Figure 3-5(a) and (b). A major cause of Cluster Mura is due to dust or particles coming into some layers of LCD panel. Poor LCD manufactory process may also produce this type of defects. We started to research the Cluster Mura detection because the Cluster Mura is the basis of Mura and the research is also partial applicable to other kinds of Mura. For example, Light Leak Mura and Around Mura can be applying the method to detect Cluster Mura.

(a) Round-type Cluster Mura

(c) Line-type Cluster Mura

(b) Detection result of (a)

(d) Detection result of (c)

Figure 3-5. Cluster Mura

In our approach, we proposed a 2-D LOG (Laplacian of Gaussian) filters The LOG filter to detect Cluster Muras. The LOG filter is designed to match the shapes of Clust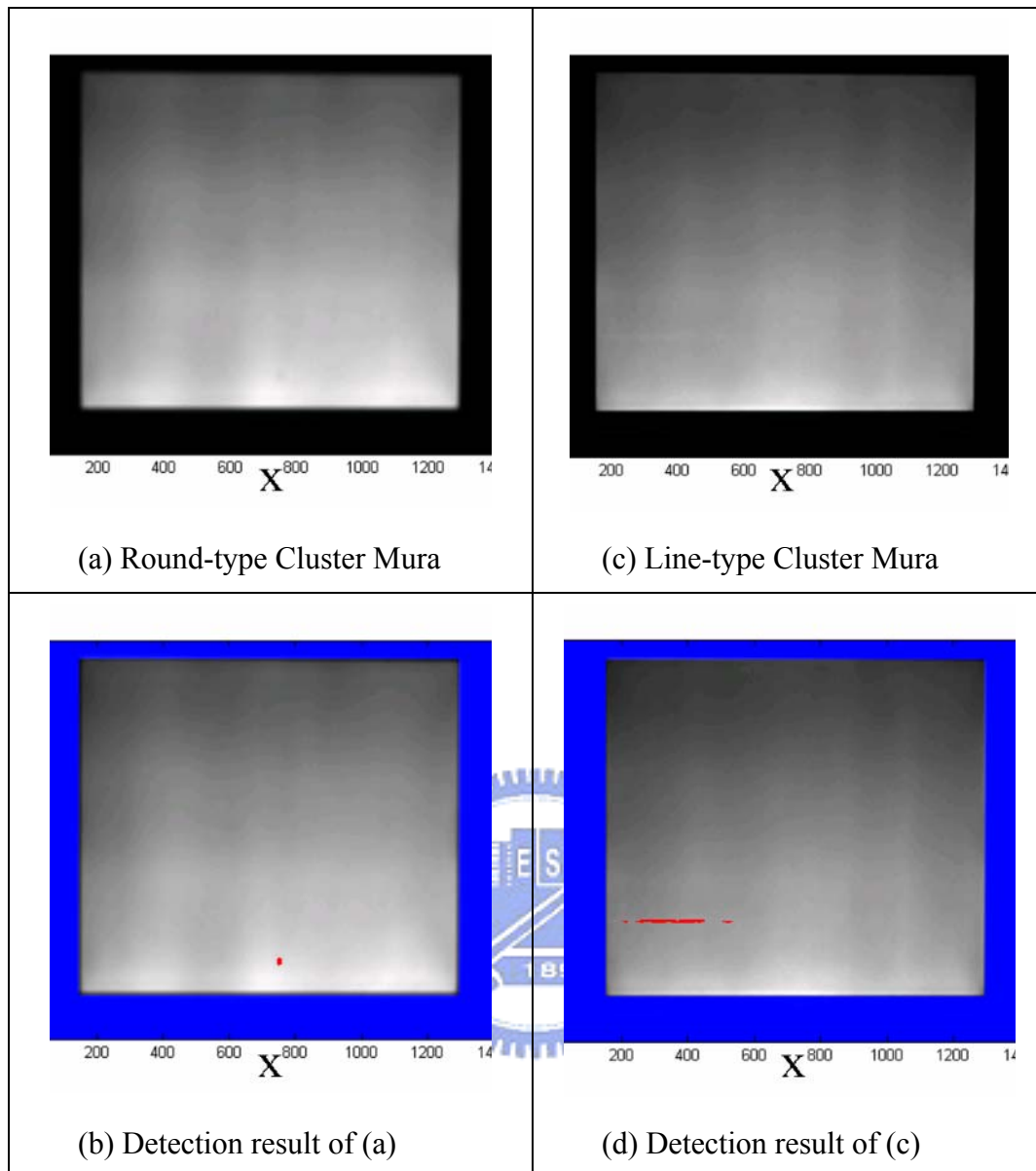er Mura, with the optimal threshold being determined based on the SEMU formula [2]. To detect round-type Cluster Muras, the round-type LOG filter is chosen to be

$$filter_{LOG}^{Round}(x,y) = \left(\nabla_{xx} + \nabla_{yy}\right)N(x,y;0,\sigma_x,\sigma_y)$$ (22)

$$= \left(\frac{2\sigma^2 - x^2 - y^2}{2\pi \cdot \sigma^6}\right) \cdot \exp\left(\frac{-x^2 - y^2}{2\sigma^2}\right)$$

, where $N(x,y;0,\sigma_x,\sigma_y) = \dfrac{1}{2\pi\sigma_x\sigma_y}e^{-\left(\frac{x^2}{2\sigma_x^2} + \frac{y^2}{2\sigma_y^2}\right)}$ denotes a 2-D Gaussian

function with zero mean and standard deviations σx and σy, respectively. If we choose

σx = σy = σ, then there is only one parameter to be assigned by the users. On the other

hand, to detect a horizontal line-type Cluster Mura, the LOG filter is chosen to be

$$filter_{LOG}^{Rectangular}(x,y) = \left(\nabla_{yy}\right)N(x,y;0,\sigma_x,\sigma_y)$$ (23)

If the ratio σ_x/σ_y of is fixed, there is only one parameter left. Similarly, to

detect a vertical line-type Mura, we can use an operator similar to (2) with ∇yy being

replaced by ∇xx.

Figure 3-6 shows these two types of LOG operator and Figure 3-5(c).
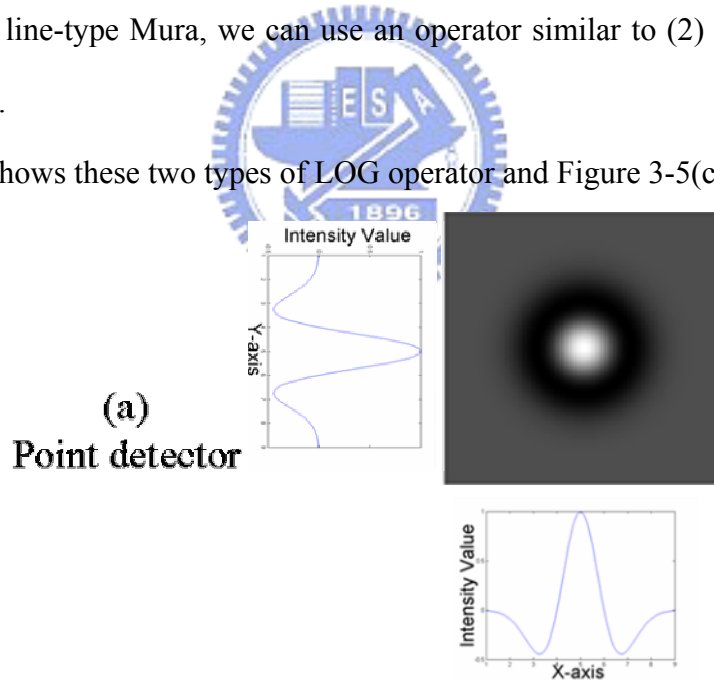
(a)
Point detector
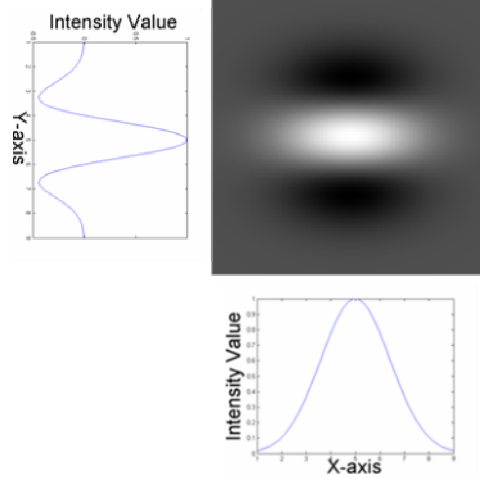
Figure 3-6. (a)   Round-type LOG operator;(b) Line-type LOG operator.

The area size of LOG filter is proportional to the standard deviation of Gaussian function. The following is the threshold selection formula used in [13]. According to SEMU [2], the Mura area is proportional to the human sensitivity of Mura. Also, the contrast between background and Mura is proportion the human eye's sensitivity.

$$\text{threshold} \equiv -\left(\frac{0.1412S}{\text{std\_dev}^{8/3}} + \frac{0.0394S}{\text{std\_dev}^2} \right); \quad S = 0.02; \tag{24}$$

Here, S means the selected Semu value and Std_dev means the standard deviation of the LOG operator. The following is the SEMU formula [2].

$$Semu = \frac{|C_x|}{C_{jnd}} = \frac{|C_x|}{(\frac{1.97}{S_x^{0.33}} + 0.72)} \tag{25}$$

Cx means the average contrast of the Mura (unit: % relative to background = 100%), Sx means the area of Mura (unit: mm2), Cjnd means the contrast of Mura at JND (unit: % relative to background = 100%).

The threshold value mentioned above will change for the LOG operators with different standard deviations. To formulate the LOG operation, we assume the intensity values of a point Mura looks like a Gaussion function. Without loss of generality, we assume the height of the Gaussian function to be 1. On the other hand, the Laplacian of

Gaussian (LOG) operator is the second derivative of a Gaussian function.

Gaussian Mura:
$$h(x,y) = \exp(-\frac{x^2+y^2}{2\sigma_1^2}) = \exp(\frac{-r^2}{2\sigma_1^2}) \tag{26}$$

LOG filter:
$$g(x,y) = \frac{\partial^2}{\partial x^2}h(x,y) + \frac{\partial^2}{\partial y^2}h(x,y) = (\frac{2\sigma_2^2 - x^2 - y^2}{2\pi \cdot \sigma_2^6}) \cdot \exp(\frac{-x^2-y^2}{2\sigma_2^2}) \tag{27}$$

After convolution, we have

$$f(x,y) = h(x,y) * g(x,y) = \frac{(k^2\sigma^2+\sigma^2)-x^2-y^2}{2\pi \cdot (k^2\sigma^2+\sigma^2)^3} \cdot e^{\frac{-(x^2+y^2)}{2(k^2\sigma^2+\sigma^2)}} \cdot 2\pi\, k^2\sigma^2 \tag{28}$$

where the standard deviation of LOG filter is σ and the standard deviation of the Gaussian Mura is K×σ.

At the center of the convolution result, we have the value

$$f(0,0) = \frac{k^2}{(k^2\sigma+\sigma)^2} \tag{29}$$

Moreover, the maximum value will appear at the places where f' = 0. Hence,

$$\frac{\partial f(x,y)}{\partial k} = 0 \Rightarrow \frac{\sigma - k^2\sigma}{(k^2\sigma+\sigma)^2} = 0 \tag{30}$$

The result indicates that f(x,y) reaches its maximum value at k = 1. This means when the standard deviation of the LOG filter is the same as the standard deviation of the Gaussian Mura, the convolution result has the maximum output. Hence, if the filter size can be matched to the size of the Cluster Mura, there will be a maximum response. On the other hand, an unmatched LOG filter will generate a response with a lower magnitude.

Let LOG std = σ and the Gaussian Mura std = σ. The maximum convolution value

will be:

$$f(x, y) = h \cdot (\frac{(2\sigma^2) - x^2 - y^2}{2\pi \cdot (2\sigma^2)^3}) \cdot \exp(-(x^2 + y^2)/2(2\sigma^2)) \cdot 2\pi\sigma^2 = \frac{h}{4\sigma^2} \qquad (31)$$
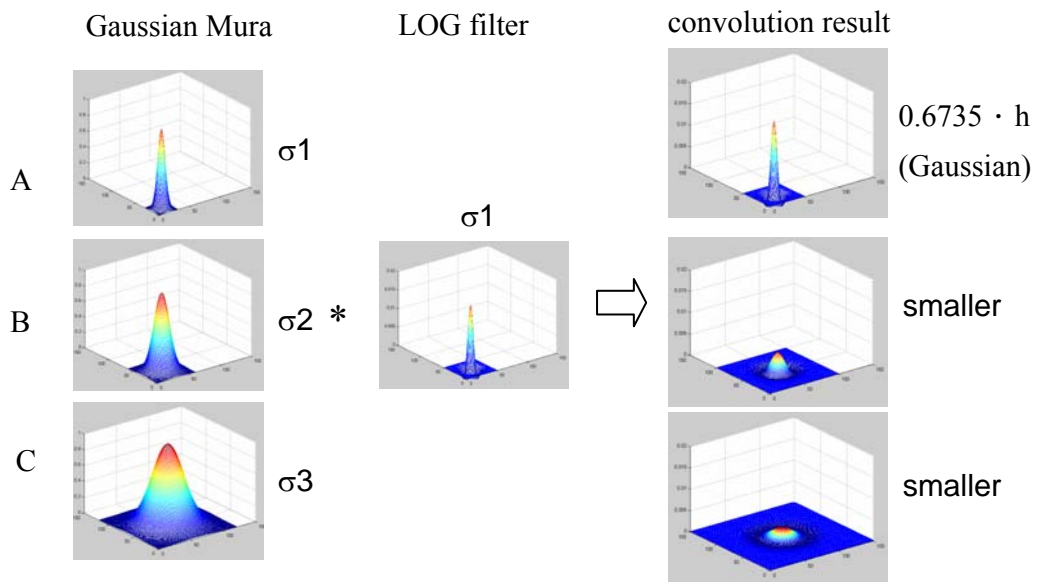
Hence, the convolution result will change as the standard deviation of the LOG filter changes. However, ff we divide the convolution result by an appropriate normalization factor, the maximum convolution value may get fixed no matter how the standard deviation of the LOG filter changes. That is, after adding the normalization factor, we have

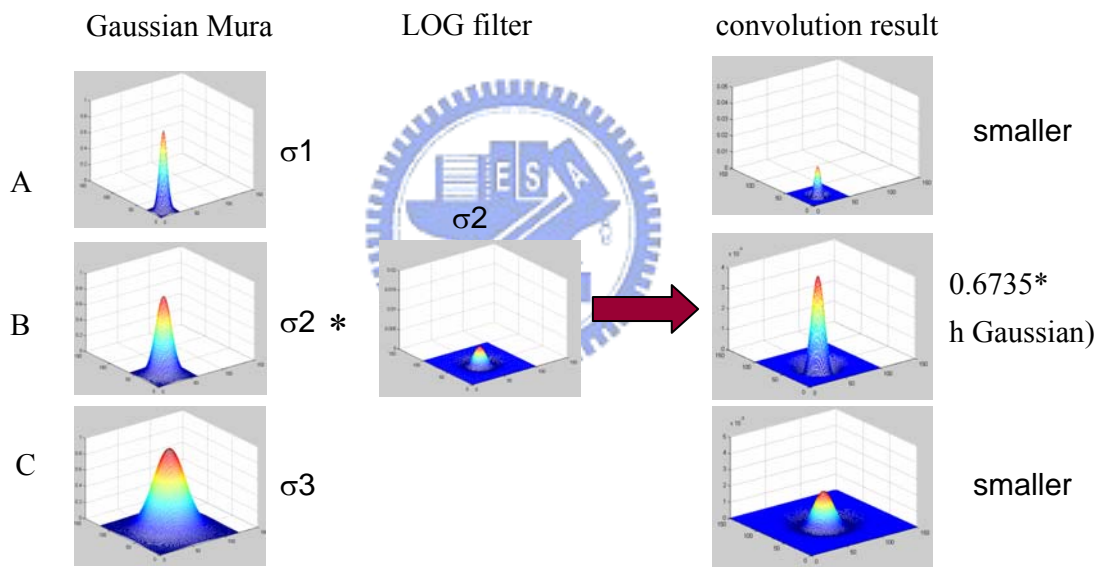$$\frac{h}{4\sigma^2} \div \frac{2 \cdot e^{(-\frac{1}{2})}}{\sqrt{2\pi\sigma^2}} = 0.6735 \cdot h \qquad (32)$$

where the normalize factor is the value used to normalize the positive summation of the LOG operator to 1.

$$k = \int_{-\sigma}^{\sigma} (\frac{\sigma_2^2 - x^2}{\sqrt{2\pi} \cdot \sigma_2^5}) \cdot \exp(-x^2/2\sigma_2^2) dx = \frac{2 \cdot e^{(-\frac{1}{2})}}{\sqrt{2\pi\sigma_2^2}} \quad (k: \text{ normalize factor}) \qquad (33)$$

Figure 3-7shows the example of convolving Gaussian Mura with a normalized LOG filter. The Gaussian Mura which matches the size of the LOG filter will have the maximum response and the maximum response value is always equal to $0.6735 \cdot h$, where h is the strength of the Gaussian Mura.

Gaussian Mura   LOG filter   convolution result

A

σ1

σ1

0.6735 · h
(Gaussian)

B

σ2 *

⇨

smaller

C

σ3

smaller

(a)

Gaussian Mura   LOG filter   convolution result

A

σ1

smaller

σ2

B

σ2 *

⟹

0.6735*
h Gaussian)

C

σ3

smaller

(b)

33

Gaussian Mura   LOG filter   convolution result

A $\sigma 1$ smaller

$\sigma 3$

B $\sigma 2$ *   smaller

C $\sigma 3$ 0.6735*

h (Gaussian)

(c)
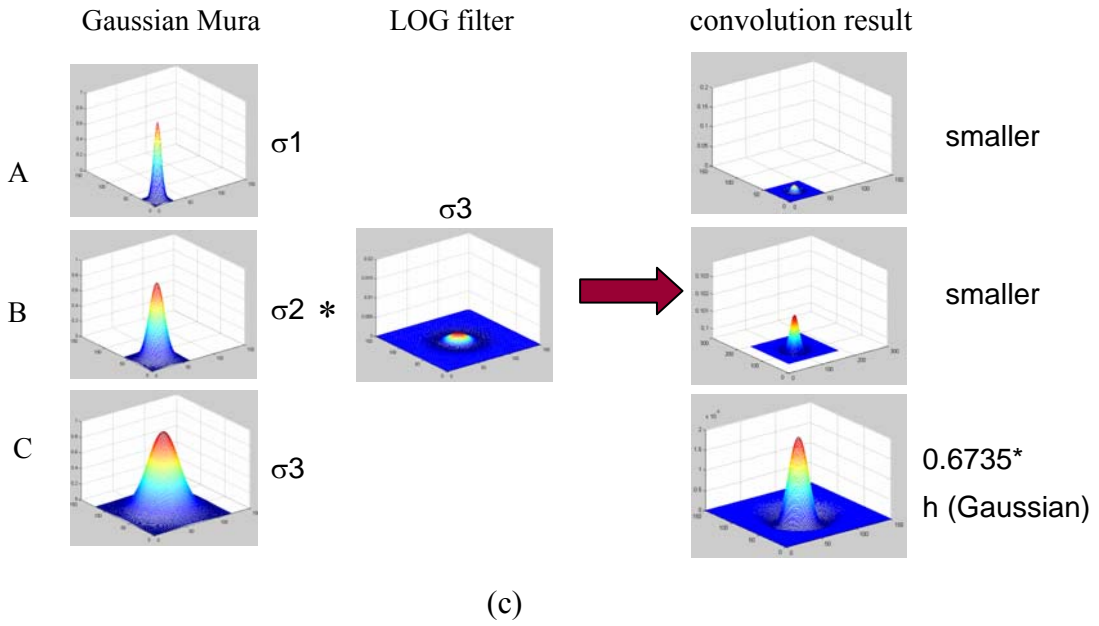
Figure 3-7 example of convolving Gaussian Mura with a normalized LOG filter

(a) a normalized LOG filter with a small σ.

(b) a normalized LOG filter with a median σ.

(c) a normalized LOG filter with a large σ.

(a)   *   (b)   =   (c)

Threshold =
0.2623· h
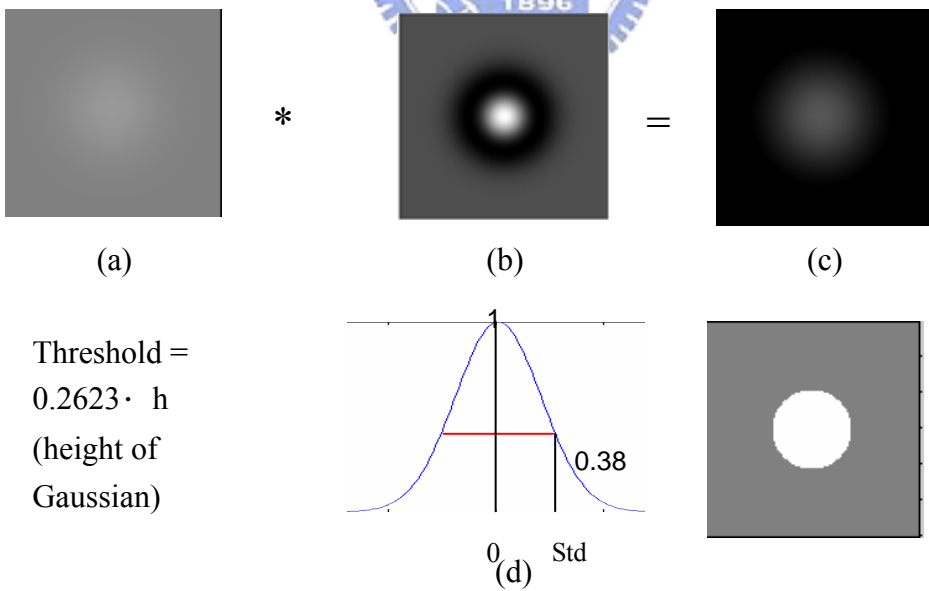(height of
Gaussian)

0.38

0

(d) Std

Figure 3-8 Example of threshold selection (a) the original pseudo Cluster Mura;

(b) matching size LOG filter (c) convolution result (d) illustration of

thresholding position (e) threshold result

The threshold of convolution result is decided by the height of the Gaussian Mura to be detected.

$$f(x,y) = h(x,y) * g(x,y) = h \cdot \frac{(k^2\sigma^2 + \sigma^2) - x^2 - y^2}{2\pi \cdot (k^2\sigma^2 + \sigma^2)^3} \cdot e^{\frac{-(x^2+y^2)}{2(k^2\sigma^2+\sigma^2)}} \cdot 2\pi k^2\sigma^2 \qquad (34)$$

The convolution result is shown in the above formula. With matching filter, k will be 1 and the maximum response will appear in x=0 and y=0. Thus, we $let \quad x = 0, y = 0$, the convolution result will be $= \frac{1}{8 \cdot \sigma^2}$. We select the standard deviation smaller than 1 to be the detected location of the convolution result. Thus, we $let \quad x = \sigma, y = 0$, the convolution result will be $= \frac{1}{4 \cdot \sigma^2} \cdot e^{\frac{-1}{4}}$. The ratio the matching maximum is

$\frac{1}{4 \cdot \sigma^2} \cdot e^{\frac{-1}{4}} / \frac{1}{8 \cdot \sigma^2} = 0.3894$, which means we can select the threshold to be 0.3894 · 0.6735 · h =0.2623 · h. In our approach, we choose h to be 0.05, which corresponds to 4-bit difference in the intensity values could be detected. Figure 3-8 shows an example of the threshold selection result.

After thresholding, the detection result will be a binary image. Some times false detection appears and we need to eliminate these falsely detected results. Figure 3-13 illustrates the example of false detection elimination based on Semu threshold. Figure 3-13 (a) show two pseudo Gaussian Muras, one in the upper-left corner, while the other in the lower-right corner. Figure 3-13 (b) shows the detection result after LOG convolution and thresholding. We can see the false detection occurs in the lower-right corner. In Figure 3-13 (d)(e)(f), the detection results are grouped into different blobs. For each blob, we evaluate its Semu value. For this example, the results are 31.6239 and

12.5487 and 1.1009, respectively. Here, we set the threshold of Semu value to be 3. Hence, these detection results with Semu value less than 3 will be removed. The final detection result is then shown in Figure 3-13 (c).
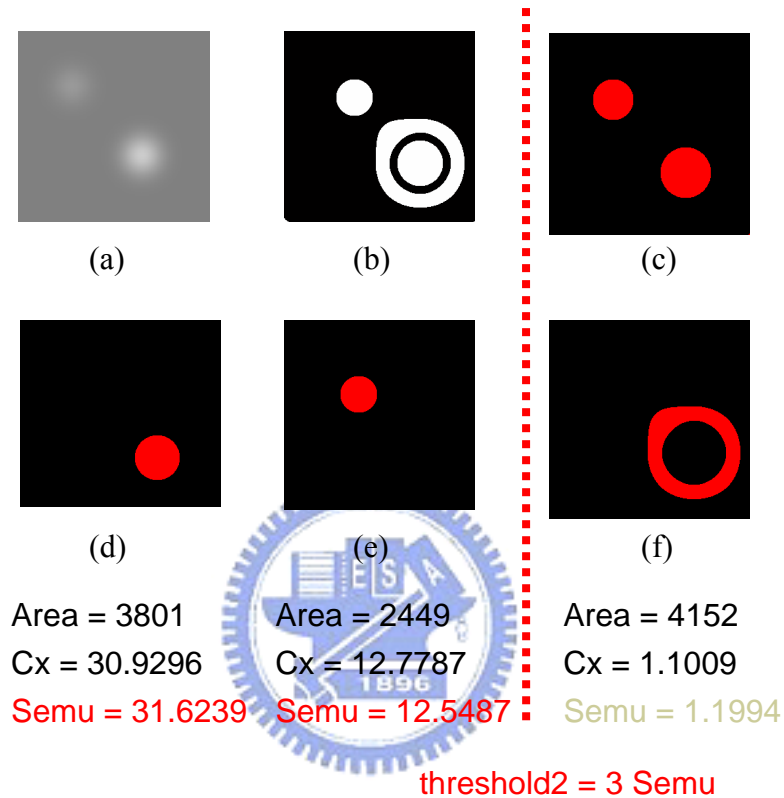

Figure 3-9 Example of Semu value thresholding. (a) original test image; (b) detection result; (c)final detection result after thresholding (d)(e)(f) evaluation of Semu value for each blob.

As mentioned before, there may be Muras of different sizes in a single LCD panel. It is not possible to detect all these Muras by using a single LOG filter. Hence, we propose the use of a bank of LOG filters of different sizes to detect Muras of different scales. In Figure 3-10, we shows five LOG filters of different sizes.
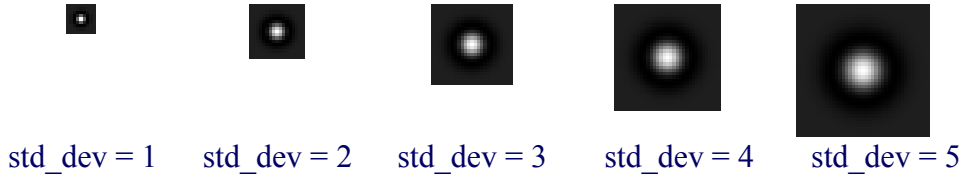
Figure 3-10 Five LOG filters of different sizes

To detect Cluster Muras of different scales, we adopt a multi-resolution approach. All these convolution results are then merged in a proper way to generate the final results. Figure 3-11 illustrates an example for the proposed multi-resolution Cluster Mura detection. Figure 3-11 (a) contains 8 synthesized Muras, with radius being 5, 10, 15, 20, 25, 30, 35, and 40, respectively. The luminance of the background is zero. For this example, we apply two LOG filters with $\sigma = 10$ and 30, respectively. As mentioned above, for each LOG filter, the convolution result will reach its maximum magnitude when the size of Mura matches to the size of the LOG filter. Figure 3-11 (b) shows the convolution result by using the LOG filter with $\sigma = 10$. It can be seen that the convolution result does reach its maximum magnitude (represented in red) at the Mura with radius 10. Figure 3-11 (c) shows a similar result when we use the LOG filter with $\sigma = 30$. Moreover, as mentioned before, both LOG filters are normalized to have their positive parts summed to 1 and negative parts summed to -1. With this normalization, when the intensity difference between the Mura and the surrounding background is kept the same, the maximum magnitude of the convolution result for different LOG filters will also be normalized to be the same.

After performing multiple convolutions with LOG filters of different scales, we merge all convolution results by calculating at each pixel the maximum magnitude of all convolution results. That is, we calculate

$$\text{result}(x, y) = \max(\text{result}_1(x, y), \text{result}_2(x, y), ...) \qquad (35)$$

where $\text{result}_i(x,y)$ denotes the convolution result at (x,y) with the use of the ith LOG

filter. Figure 3-11(d) shows the final result based on (5). Figure 3-11(e)~(g) show the detection results of Figure 3-11 (b)~(d) by setting the threshold to be 100. As expected, it can be seen that the smaller LOG filter detects only small Muras, while the larger LOG filter detects only large Muras. However, with the proposed multi-resolution approach, all sizes of Mura defects can be correctly detected.
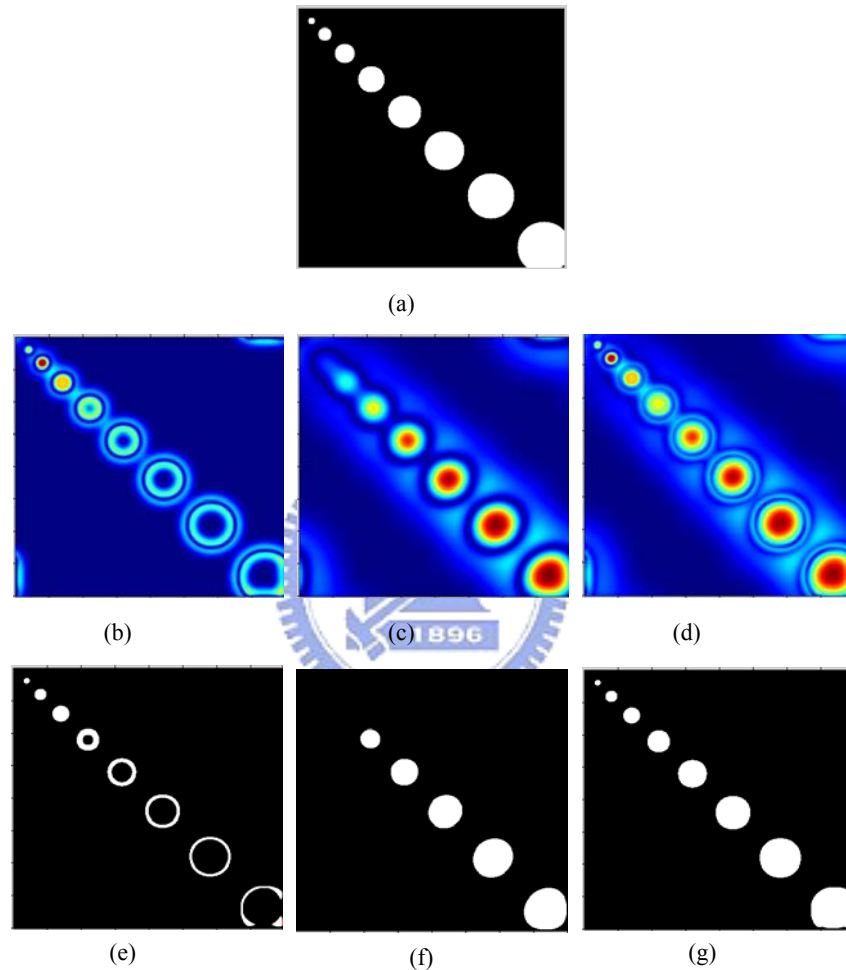

(a)

(b)   (c) 1896   (d)

(e)   (f)   (g)

Figure 3-11 Multi-resolution Cluster Mura detection

(a) test image; (b) result by using an LOG filter with σ =10; (c) result by using an LOG filter with σ =30; (d) maximization of (b) and (c); (e)~(g) detection results of (b)~(d), respectively, with threshold =100.

Figure 3-12 shows the multi-resolution detection result of Cluster Mura. It can be seen that the detection results are pretty consistent with respect to the original image.

(min., max.) = (500, 700)

(min., max.) = (300, 500)
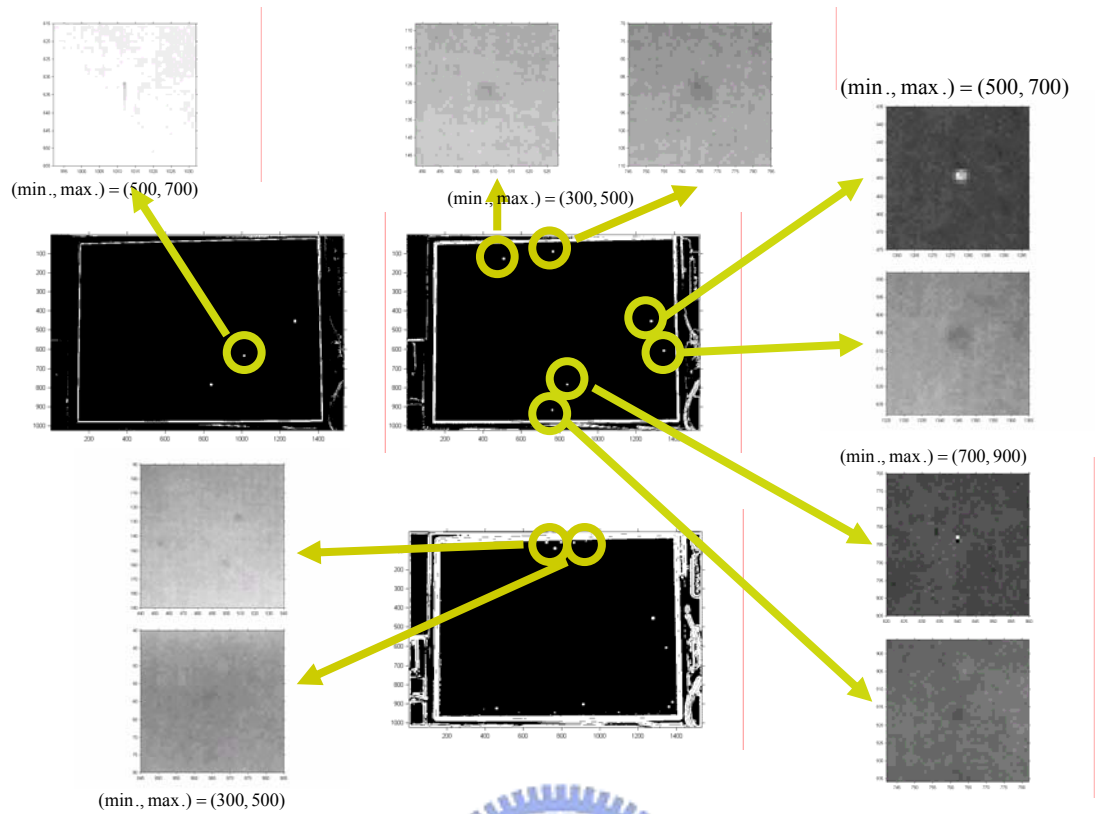
(min., max.) = (300, 500)

Figure 3-12 Multi-resolution detection result of Cluster Mura

Even though the method proposed here is quite effective in detecting Cluster Muras, the execution time of spatial convolution could be a problem. In the detection of Cluster Muras, we need to inspect Muras of different sizes. As we increase the size of the LOG operator to detect Cluster Muras of larger size, the computation load of the convolution operation increases exponentially. To deal with this kind of problem, we convert the operation from spatial domain to frequency domain. In theory, convolution of two digital patterns in the spatial domain is equivalent to multiplication of their counterparts in the frequency domain. More explicitly, we have

$$\Im\{f(x,y)*g(x,y)\} = \Im\{f(x,y)\}\cdot\Im\{g(x,y)\}$$ (36)

or

$$f(x,y)*g(x,y) = \Im^{-1}\{\Im\{f(x,y)\}\cdot\Im\{g(x,y)\}\}$$ (37)

39

where * denotes the spatial convolution operation and $\Im\{.\}$ denotes the Fourier transform operation. Hence, to perform the convolution operation, we may compute the Fourier transforms of the original image and the LOG operator first, multiply their transforms together, and then perform inverse Fourier transformation over their multiplication product to get the final convolution result. Note that we only need to perform the Fourier transform of the original image once. To detect Cluster Muras of different sizes, we only need to multiply the Fourier transform of the original image with the Fourier transforms of different LOG filters. These multiplication products are then converted back to the spatial domain, respectively.

Figure 3-13 illustrates an example of this process. Figure 3-13 (a) shows the FOS image of an LCD panel and Figure 3-13 (b) shows its Fourier transform. Here, we apply FFT (Fast Fourier Transform) for the computation of Fourier transform. Figure 3-13(c) shows the Fourier transform of a round-type LOG filter with $\sigma x = \sigma y = \sigma = 1$. Figure 3-13(d) shows the product of Figure 3-13(b) and (c). After computing the multiplication product, we perform inverse Fourier transform to get the corresponding convolution result. A threshold is then selected to detect Cluster Muras. Figure 3-13(e) shows a zoomed image of the red rectangle area marked in Figure 3-13(a). Figure 3-13(f) shows the corresponding detection result. These detected pixels are grouped into blobs. Based on the Semu formula [2], we further check the semu value of these detected blobs to determine whether these blobs are perceivable to human eyes.
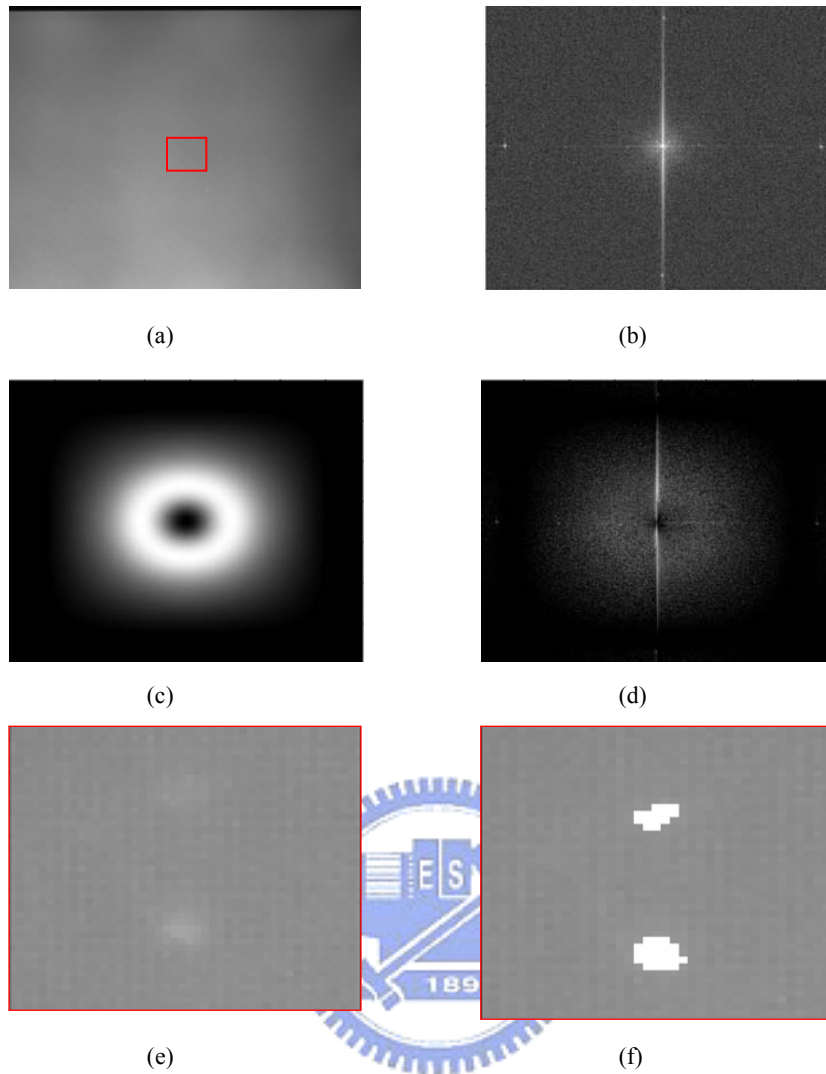
Figure 3-13 Example of Cluster Mura detection; (a) original image; (b) FFT of the original image; (c) FFT of an LOG filter; (d) product of (b) and (c); (e) zoomed image of the original image; (f) detection result

3.3 Inspection of Light Leak Mura

Light Leakage Muras usually appears at the boundary regions of an LCD panel. An ideal LCD panel should have no visible bright area around the boundaries of the panel if the screen is in fully dark. However, Light Leakage may occur at the boundaries due to misalignment during manufacturing. The non-uniform distribution of brightness enhancement film in the boundary region may also produce this kind of Mura defect.

Figure 3-14 (a) shows an example of Light Leakage Mura. We can easily see that both the upper side and the bottom side of the FOS image appear brighter than the other regions. Figure 3-14 (b) shows the 1-D intensity profile along the red vertical line in Figure 3-14(a). The intensity values at both ends are much higher than that in the center. Figure 3-14(c) and Figure 3-14 (d) show the 1-D intensity profiles along the two red horizontal lines in Figure 3-14 (a). It can be seen that the intensity value across the center part is roughly flat, while the intensity value along the bottom boundary changes quite dramatically.

(a) (b)

(c) (d)

(e)
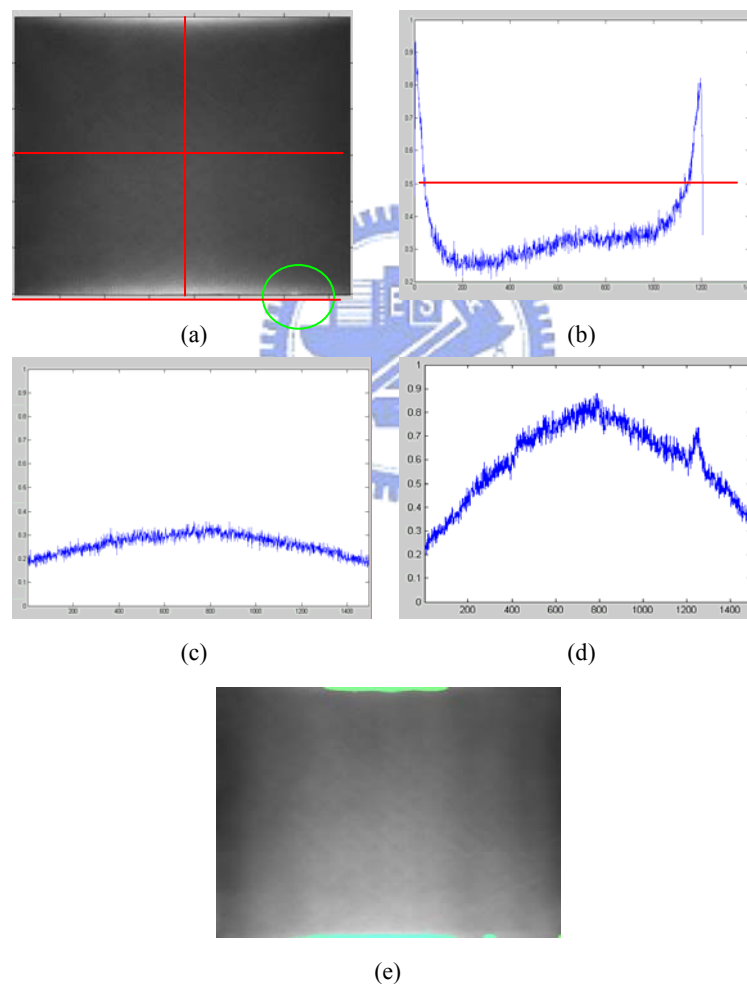
Figure 3-14. (a) FOS image with Light Leakage Muras; (b) 1-D intensity profile along the vertical red line in (a); (c) 1-D intensity profile along the central horizontal line in (a); (d)1-D intensity profile along the bottom horizontal line in (a); (e) detection result.

To detect Light Leakage Muras, we also adopt the aforementioned LOG filter that has been used in the detection of Cluster Muras. However, since Light Leakage Muras always occur at boundaries of the FOS image, we need to manipulate the boundary regions properly before we apply the LOG operator. As shown in Figure 3-15(b), above the top boundary of the FOS image, we pad a mirror image of that part. After the padding, a Light Leakage Mura appears just like a line-type Cluster Mura and we can simply apply a line-type LOG filter as shown in Figure 3-15(c) to detect it. The process would be the same as that in detecting Cluster Muras. The detection result of Figure 3-14(a) is shown in Figure 3-14(e).

(a)

(b)

(c)

(d)
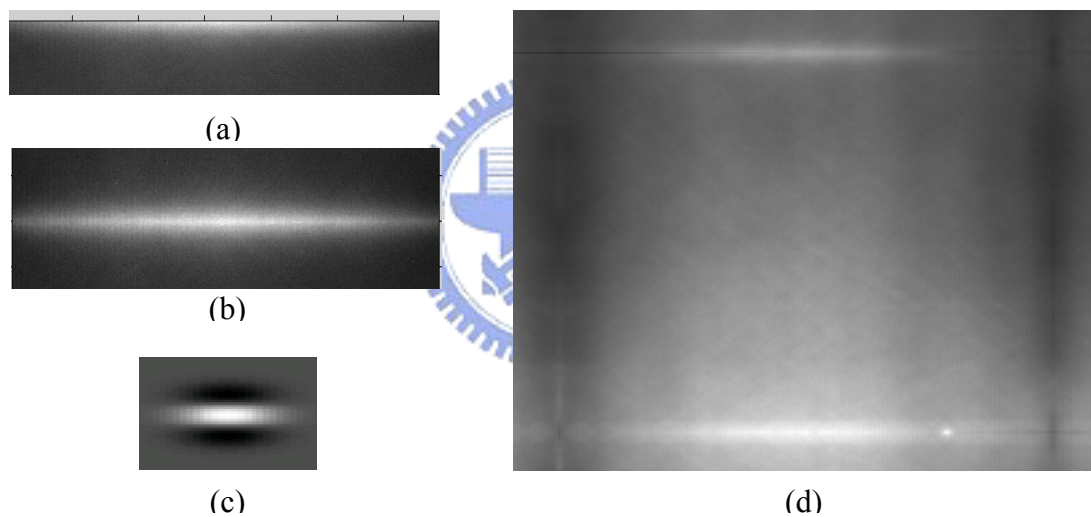
Figure 3-15 (a) Top boundary area of Figure 3-14 (a); (b) padded on the top of (a) with a mirror image; (c) applied line-type LOG filter. (d) padded image

3.4 Inspection of Rubbing Mura

During the manufacturing of LCD panels, the rubbing process is a process to control the arrangement of liquid crystals. However, during this rubbing process, dust or particles may cause Rubbing Muras. Poor rubbing process or polluted rubbing cloth may also cause this kind of defects. Figure 3-16(a) shows a typical Rubbing Mura on the FOS image of an LCD panel. These rubbing lines appear along the diagonal direction. Because these rubbing lines appear as a periodic pattern, we may apply frequency-domain analysis to the extraction of Rubbing Muras.

(a)   (b)

(c)   (d)

(e)
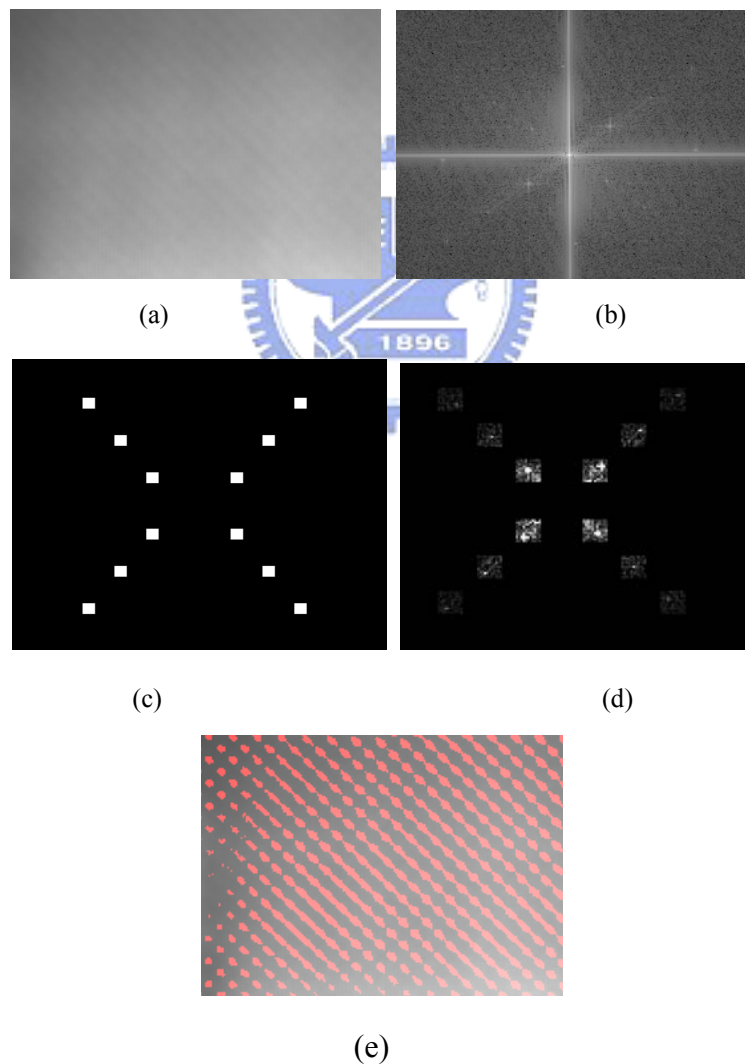
Figure 3-16. (a) FOS image with Rubbing Mura; (b) FFT of (a); (c) frequency mask; (d) masked frequency components; (e) detected Rubbing Mura.

Figure 3-16 (b) shows the FFT of the FOS image with Rubbing Mura. The center of Figure 3-16 (b) represents the dc component and the two axes represent the frequency axes along the vertical and horizontal directions. Due to the existence of Rubbing Mura, there appear a few bright points in Figure 3-16 (b) that correspond to the strong periodic components in the FOS image. In our experiments, Rubbing Muras tend to appear at the same frequency. With this observation, we presume the same manufacturing process will produce the same type of Rubbing Mura. Hence, we explicitly design a frequency mask as shown in Figure 3-16(c) to sift out unnecessary frequency components. Moreover, in the design of the frequency mask, we also preserve the 2nd and 3rd harmonic components. Figure 3-16 (d) shows the masked frequency contents. If we transform the masked frequency components back to the spatial domain via inverse FFT, we can get the red pattern as shown in Figure 3-16(e). This pattern does correspond to the Rubbing Mura in Figure 3-16(a). Hence, to detect Rubbing Muras, we may simply check whether there are distinct components in the masked frequency components. Here, we check the sum of power to detect the existence of distinct components. In Table 1, we show the comparison between the JND (Just Noticeable Difference) value and the sum of power of the masked frequency components. These subjective JND values are determined by professional LCD panel inspectors, who had been well trained to inspect the visual quality of LCD panels. A Mura with "JND-value =1.5" indicates that the contrast of that Mura is about 1.5 times of the JND level, subjectively. Table 1 indicates that the JND-value of a Rubbing Mura is basically proportional to the power sum. As a result, we can select a threshold, shown as the red line in Table 1, to determine whether there is a Rubbing Mura in the FOS image of an LCD panel. Note that the thresholding is performed in the frequency domain and there is no need to convert the masked frequency components back to the spatial domain.

Table 4. JND value inspected by inspectors versus power sum in the masked frequency components

LCD number	JND value by inspector	Sum of power in frequency domain
LCD1		16801
LCD2		18544
LCD3		30912
LCD4		33492
LCD5		41728
LCD6		43381
LCD7		58281
LCD8	1.8	129056
LCD9	2.2	155356
LCD10	1.8	169928
LCD11	1.7	176191
LCD12	2.1	195643
LCD13	2.1 L92 1.8	274746
LCD14	2.4 L92 2.2-2.3	275137

Threshold (dotted red line above LCD8)

3.5 Inspection of V-band Mura

V-band Mura appears as a wide, vertical stripe with different brightness with respect to the background. The cause of V-band Mura usually comes from non-uniform thickness of components, such as non-uniform thickness of glasses in the cell unit. This type of Mura spreads over a large area. Hence, it is difficult to detect V-band Muras based simply on local operator. To detect V-band Mura, we check the variation tendency of the projected 1-D intensity profile. Figure 3-17 (a) shows an FOS image. We first vertically project the 2-D image data into a 1-D intensity profile, shown as the blue dotted line in Figure 3-17 (b). In the projected profile, significant intensity deviations

indicate the existence of V-band Muras. To detect large intensity deviation, we analyze the variation tendency of the projected profile by checking the profile curvature. Here, we adopt the zero-crossing points on the profile curvature to indicate the turning points of variation tendency. Based on these zero-crossing points, a 2nd-order curve fitting is performed to generate a smooth approximation of the projected profile, shown as the cyan line in Figure 3-17 (b). Figure 3-17(c) shows the difference between the smooth approximating profile and the original profile. The difference is smoothed by Gaussian filter to suppress noise. Red points indicate local minimums while green points indicate local maximums. To determine whether there is a visible V-band Mura, we calculate at each local extreme the intensity difference between that extreme and its adjacent local extremes, indicated as the red line in Figure 3-17(c). This intensity difference indicates how serious a local deviation is, as indicated in Figure 3-17 (d). If the difference is above a pre-selected threshold, that local deviation is detected as a V-band Mura. In our experiments, the threshold is set to be 0.015, empirically. Figure 3-17(e) shows the final detection result, with the cyan box indicating the area of the detected V-band Mura.

(a)   (b)

(c)   (d)

(e)
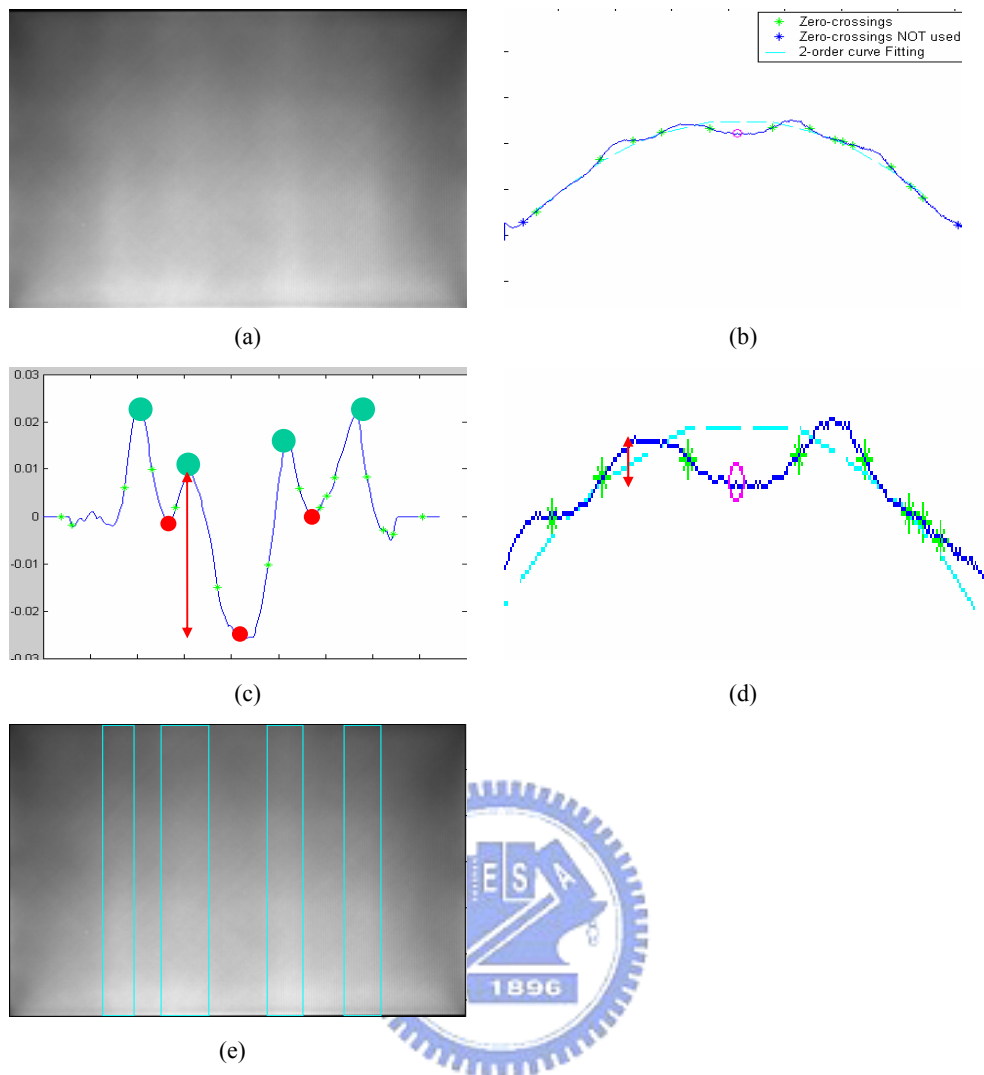
Figure 3-17 Example of V-band Mura detection (a) original FOS image; (b) projected 1-D profile, zero-crossing points, and fitted curve; (c) difference between the 1-D projection and the fitted curve; (d) illustration of intensity deviation;(e) detection result.

Picture capture environment of Light Leakage Mura

Light Leakage Muras appear brighter than the surrounding region. If the LCD displays high luminance, the leakage light might not be visible. Hence, Light Leakage Muras should be observed when the LCD panel is displayed in low luminance. In our inspection procedure, the pattern generator normally displays L92 luminance and

most defects can be observed under this luminance situation, including bright Mura and dark Mura. However, L92 is too bright for the inspection of Light Leakage Muras. In this case, L0 is a better choice. Figure 3-18 shows two images under different test situations. Figure 3.5.8 (a) shows the LCD image captured in L92, while Figure 3-18 (b) shows the same LCD image captured in L0. Figure 3-18 (c) shows the 1-D vertical projection profile in L92, while Figure 3-18 (d) shows the 1-D vertical projection profile in L0. We can easily see that the peak in Figure 3-18 (d) is much higher than that in Figure 3-18 (d). Hence, it is much easier to detect Light Leak Muras based on Figure 3-18(d). Thus, in our inspection procedure, Light Leakage Muras are to be inspected under L0.

(a) (b)

(c) (d)
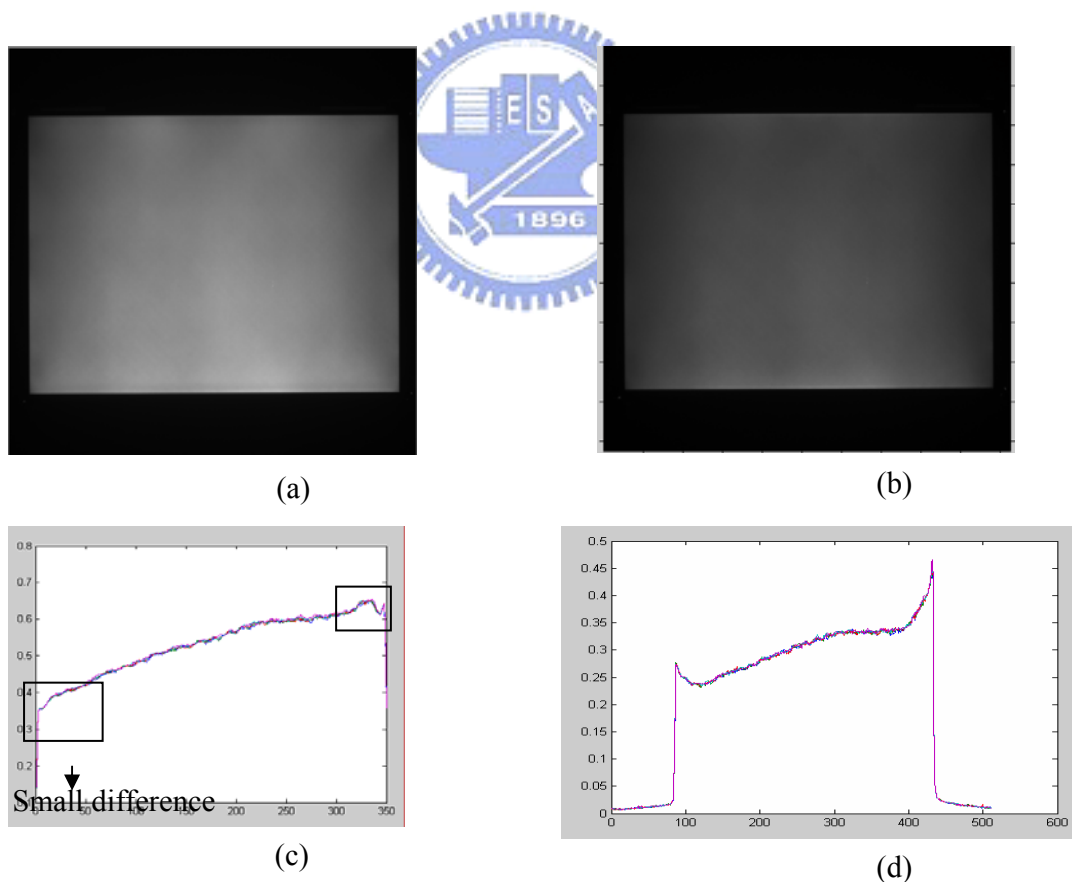
Figure 3-18 Different test luminance of Light Leak Mura. (a) Captured image in L92; (b) Capture imaged in L0; (c) vertical projection profile of (a); (d) vertical projection profile of (b).

49

Chapter 4 Experimental Results

4.1   Detection results of Light Leak Muras

In this section, Light Leak Mura detection results are shown, together with their original images.
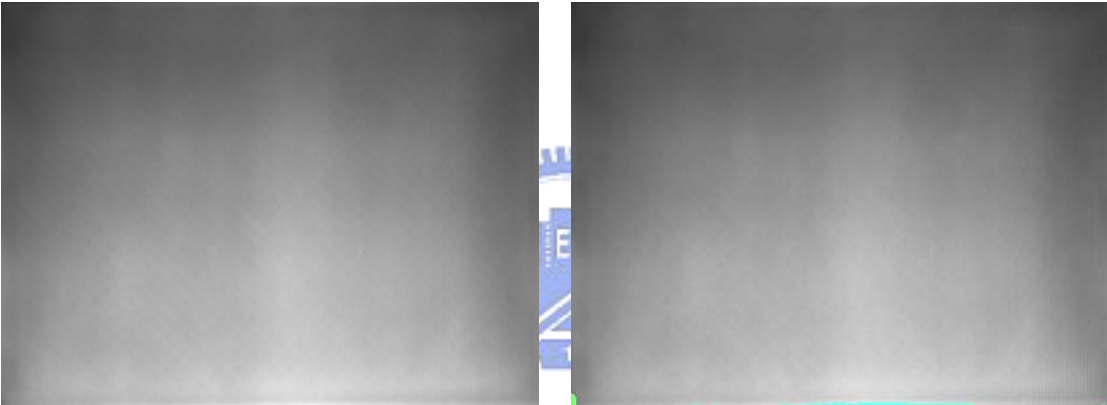
LCD panel NO.1
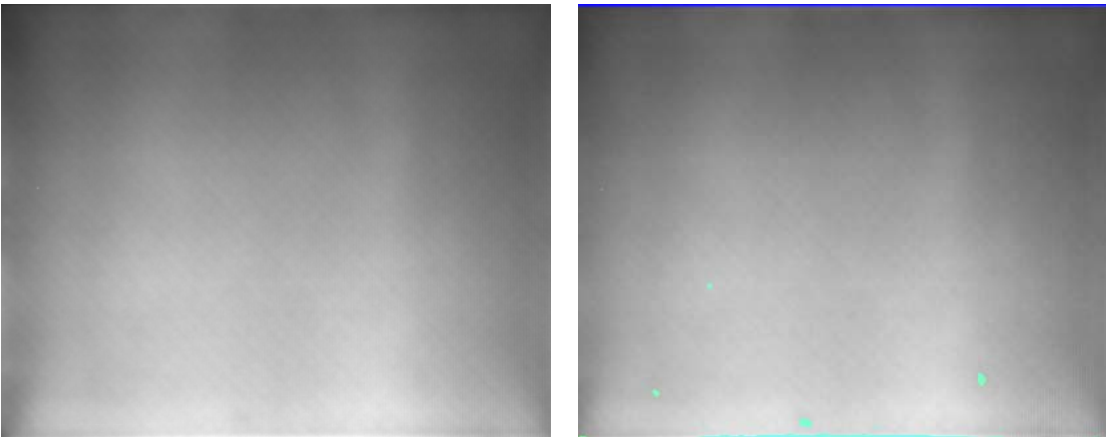
LCD panel NO.2
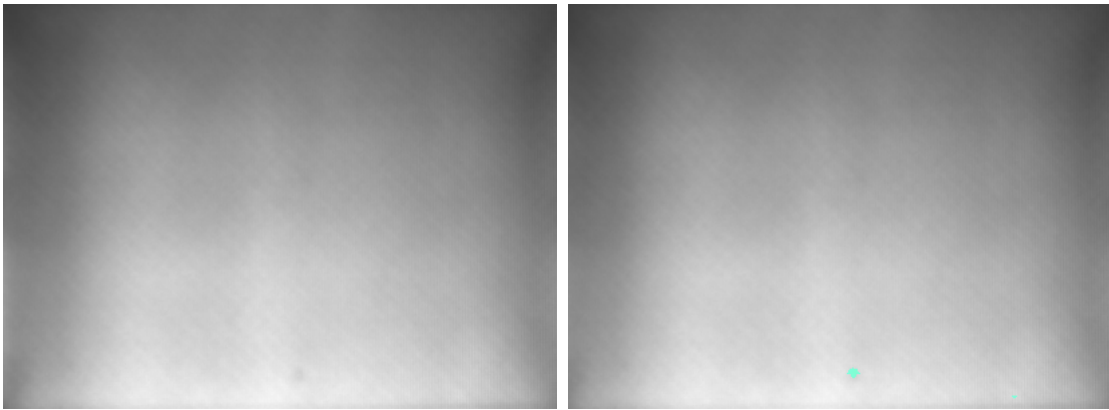
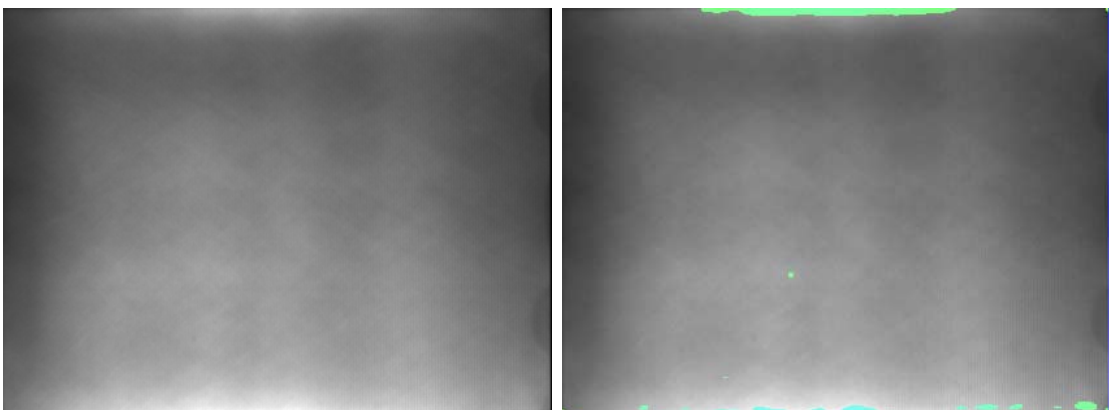LCD panel NO.3
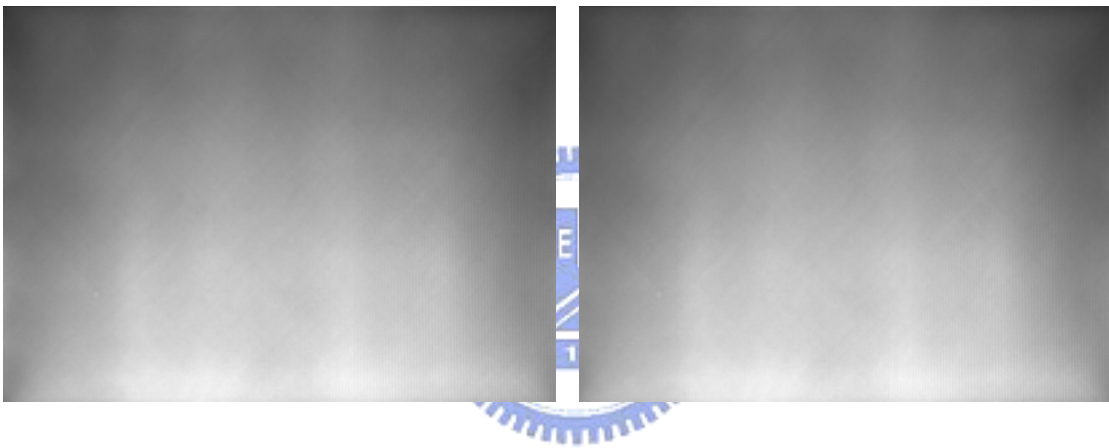
LCD panel NO.4
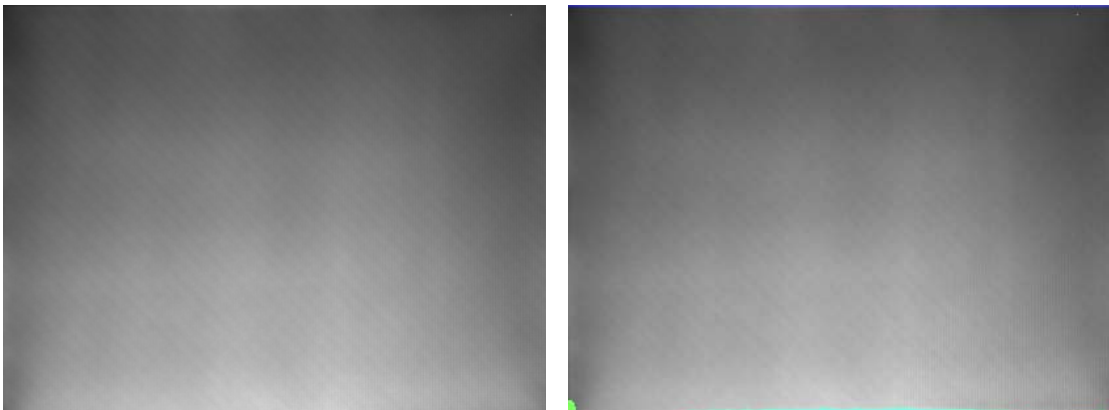
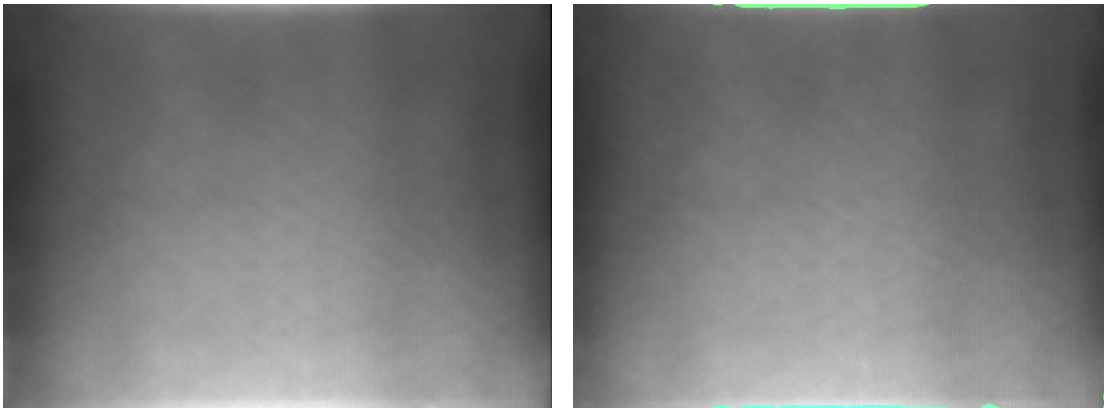

LCD panel NO.5
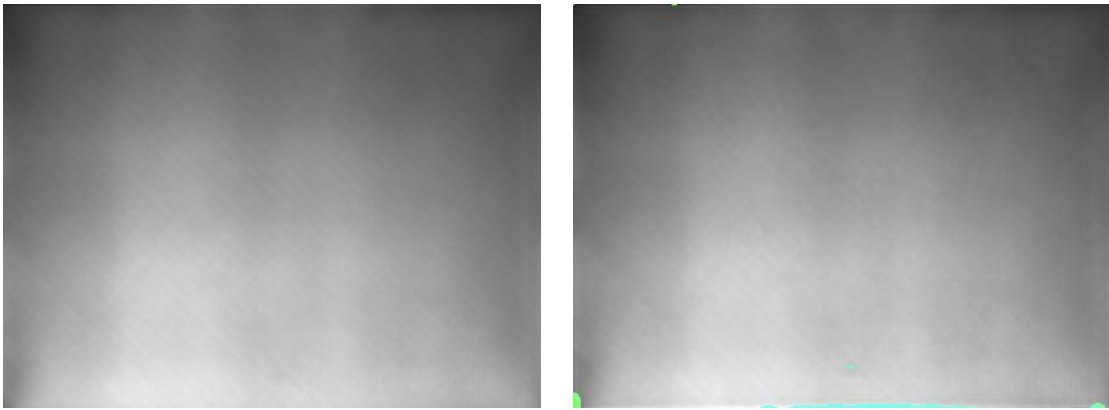
LCD panel NO.6
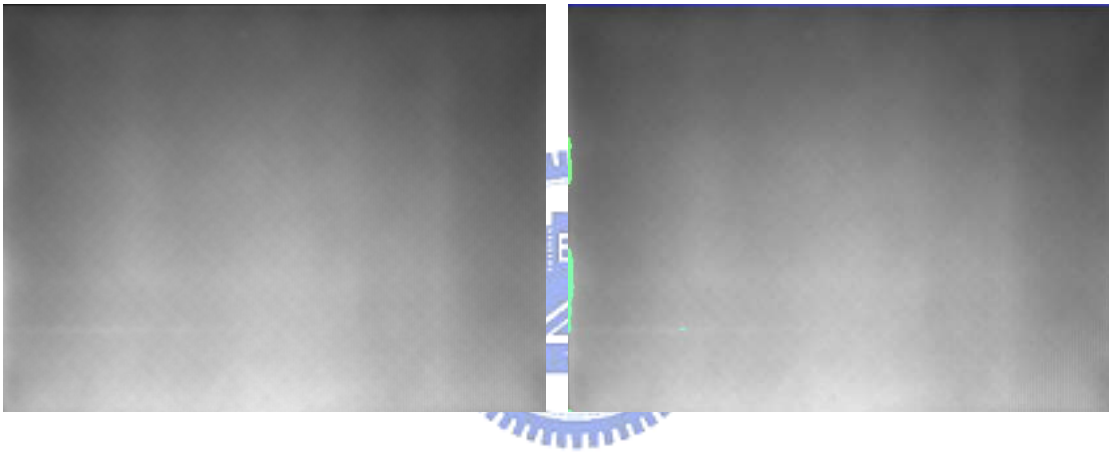
LCD panel NO.7

LCD panel NO.8

LCD panel NO.9

Figure 4-1 Light Leak Mura detection result; threshold = 0.02, std of LOG =6
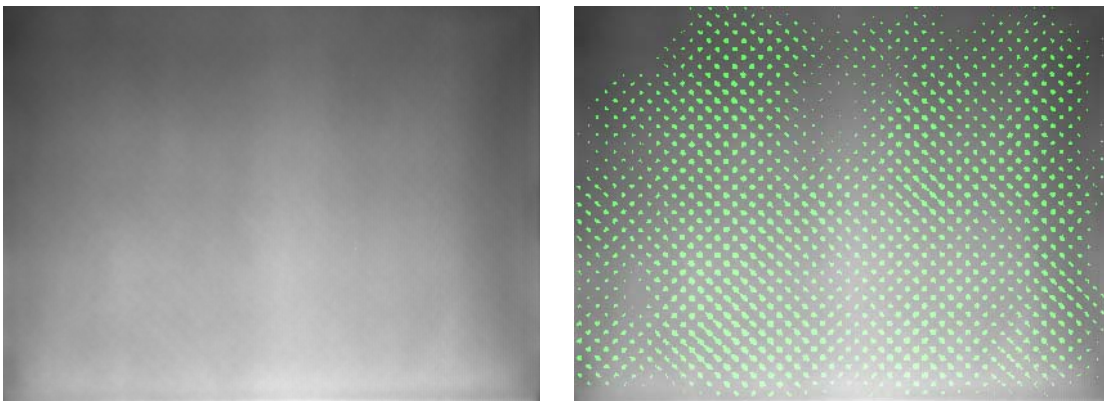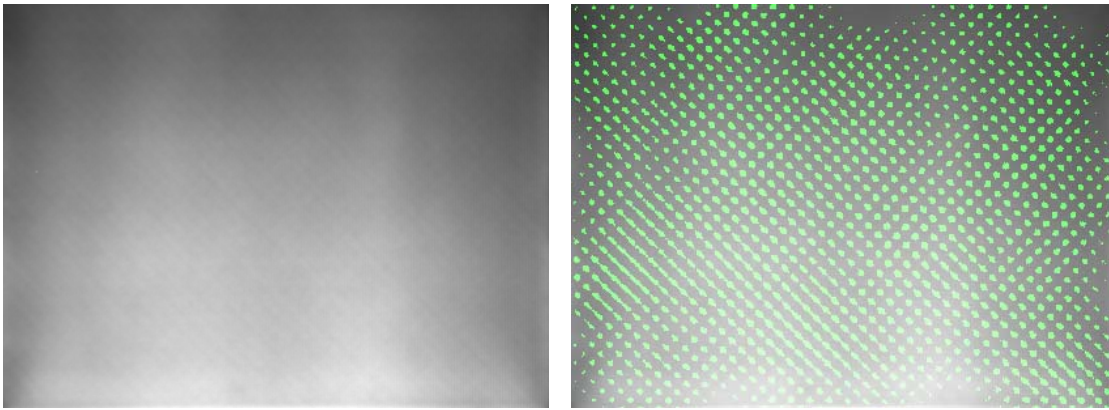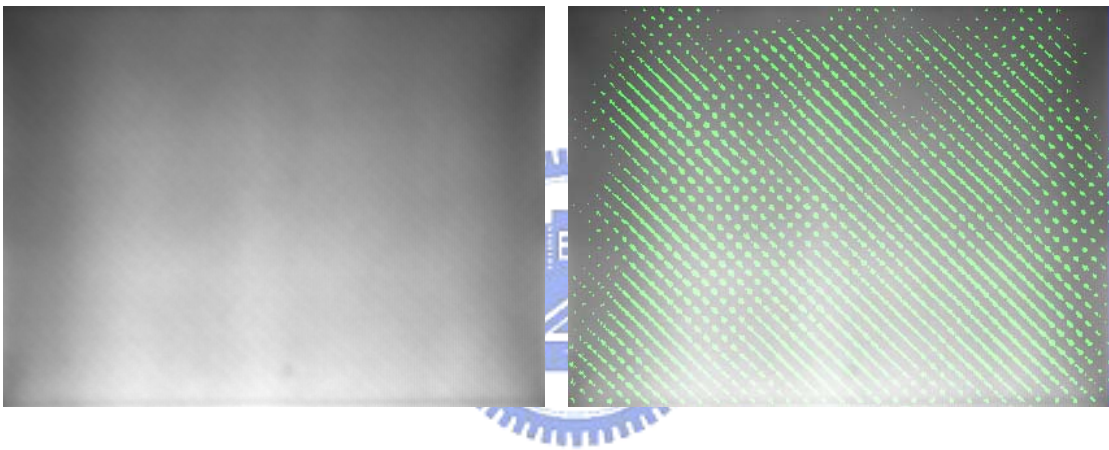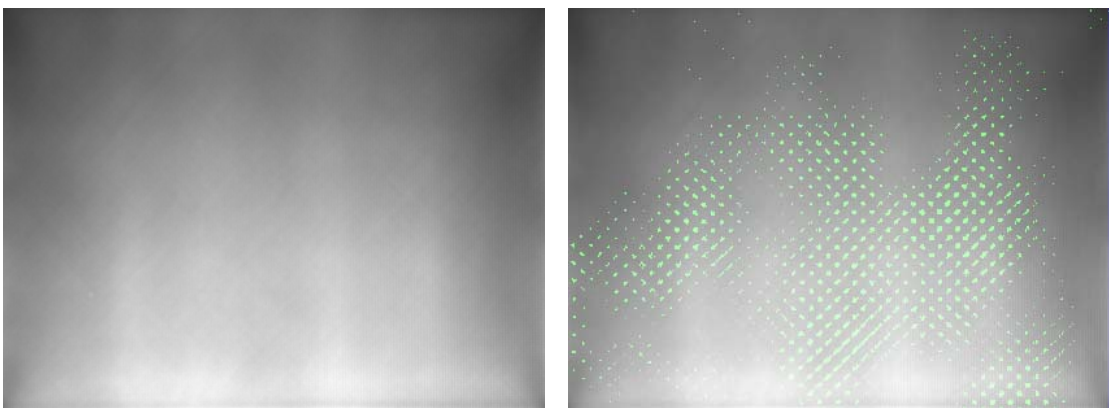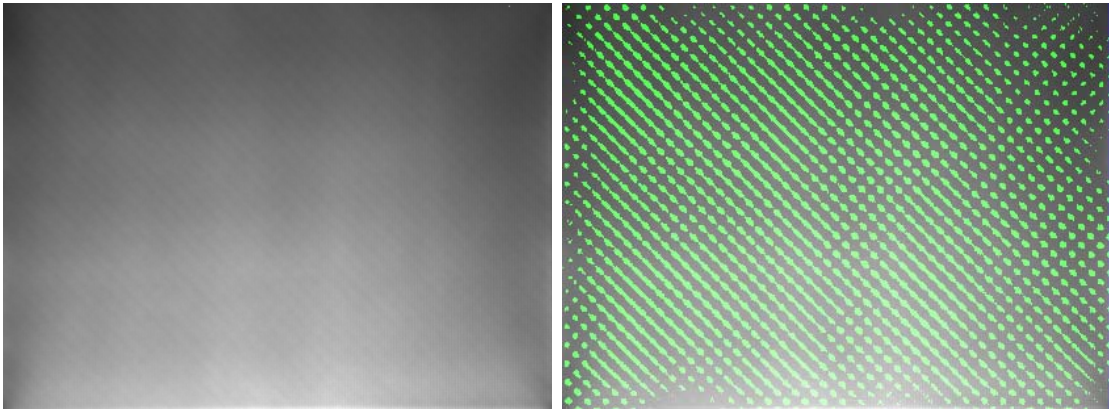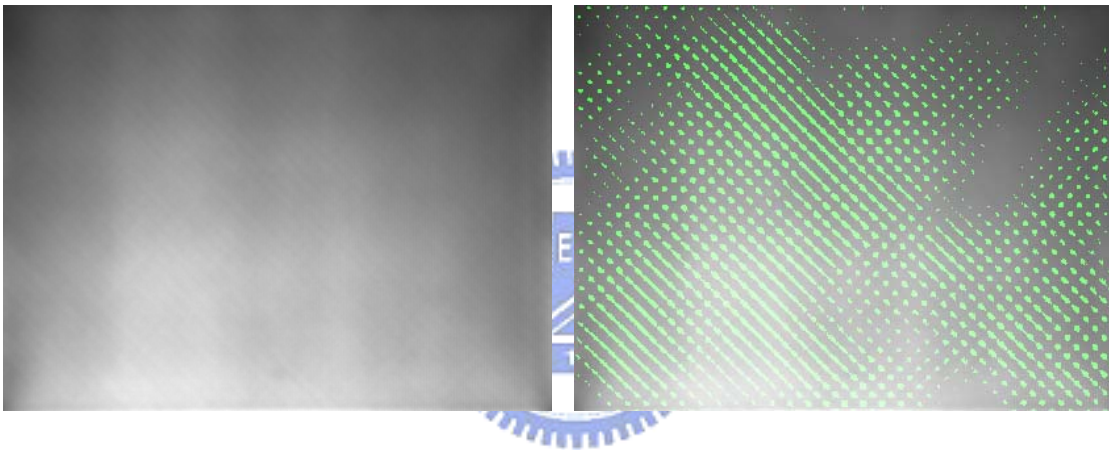
Left: original images;

Right: detection results.

4.2　　**Detection Results of Rubbing Muras**

In this section, Rubbing Mura detection results are shown, together with their original images
.

LCD panel NO.1

LCD panel NO.2
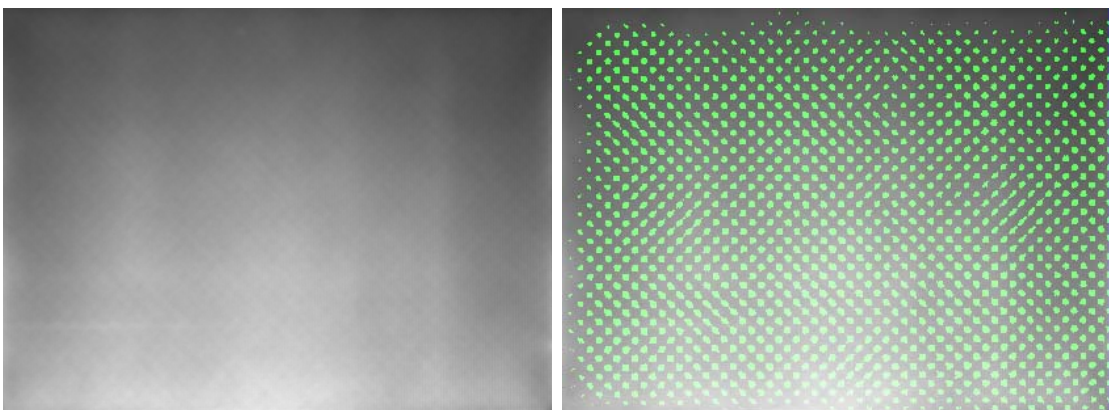

LCD panel NO.3

LCD panel NO.4

LCD panel NO.5

LCD panel NO.6

LCD panel NO.7

LCD panel NO.8

LCD panel NO.9

Figure 4-2 Rubbing detection result; threshold = 0.002

Left: original images;

Right: detection results

4.3 Detection results of V_band Muras

In this section, V-band Mura detection results are shown, together with their original images.

LCD panel NO.1

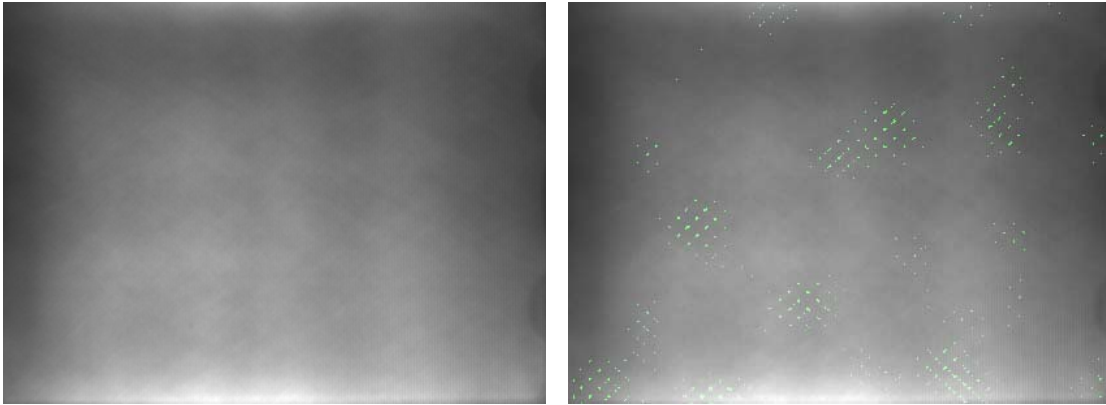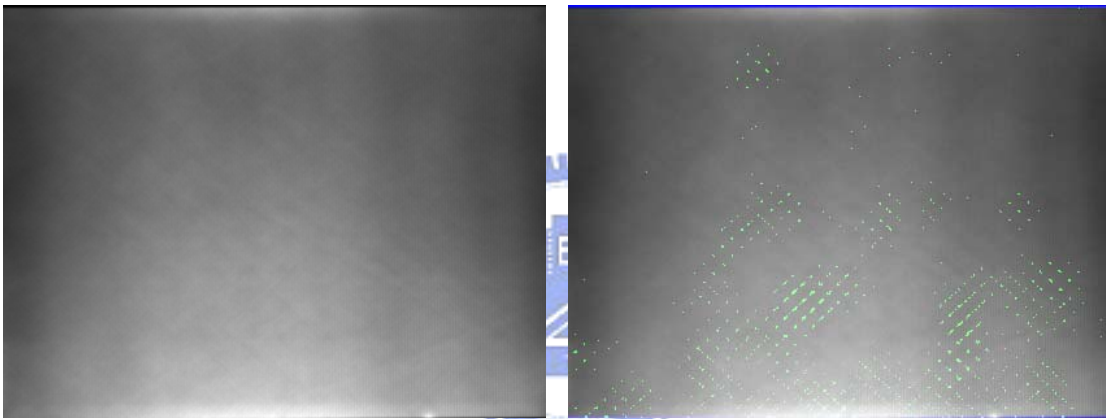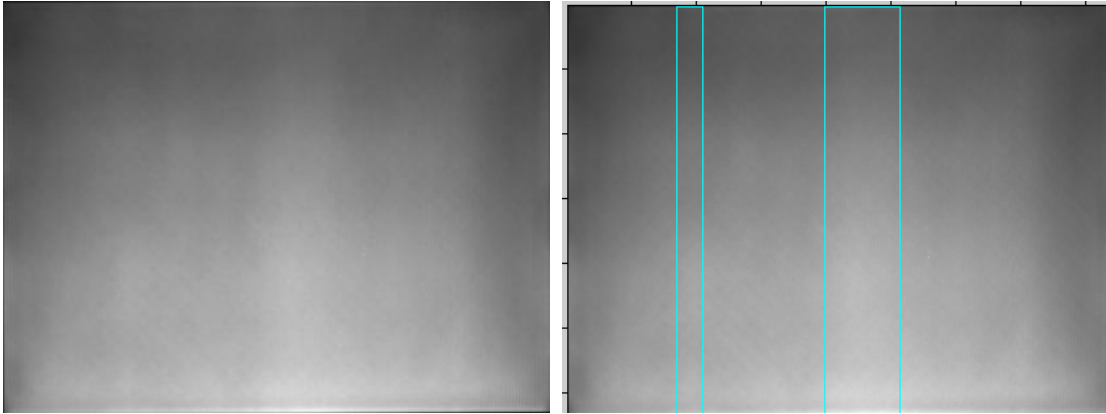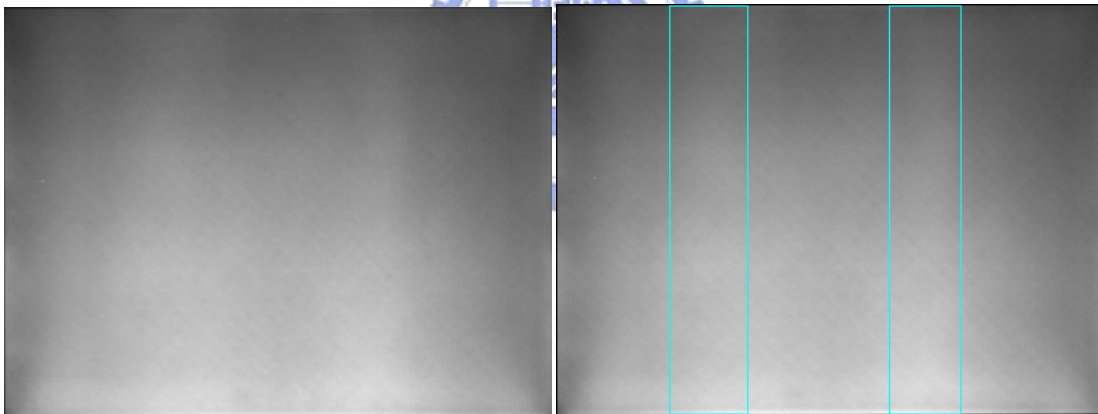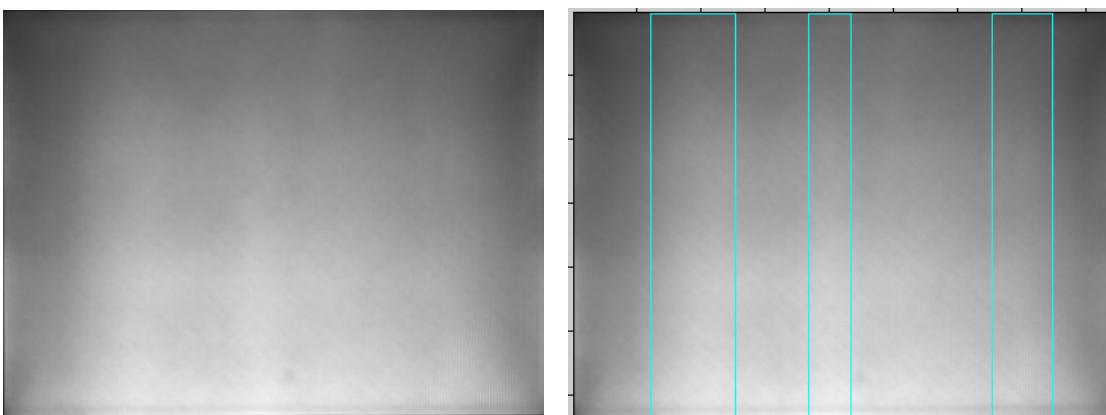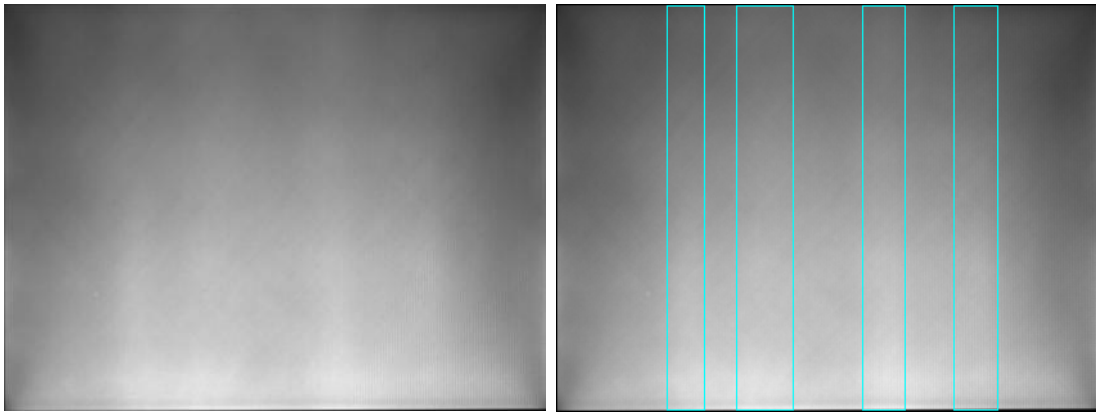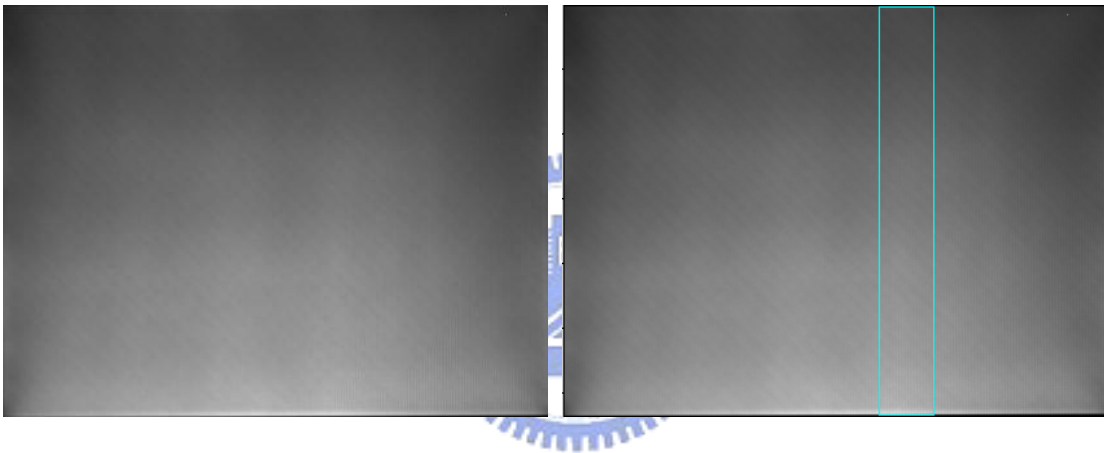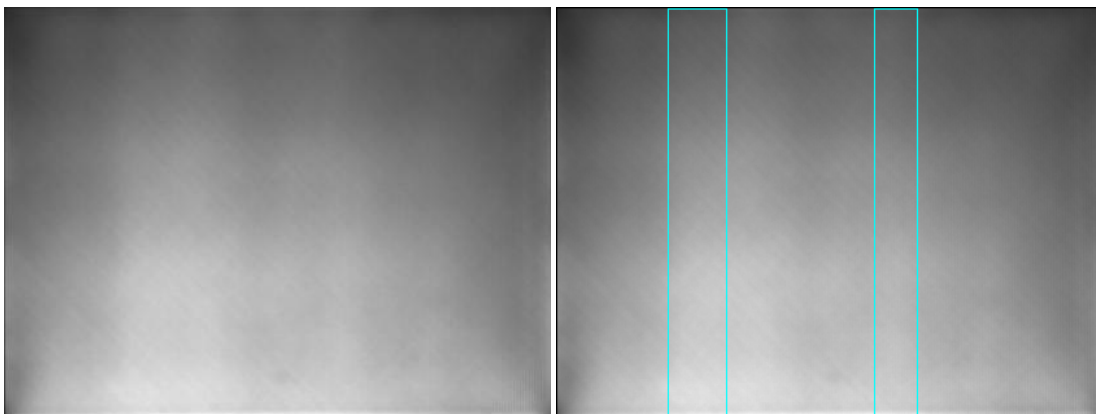
LCD panel NO.2

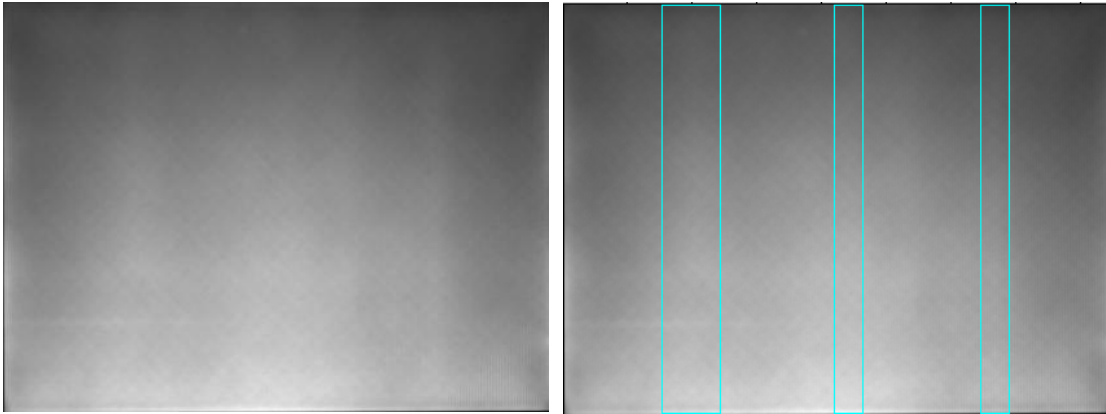LCD panel NO.3

LCD panel NO.4

LCD panel NO.5

LCD panel NO.6
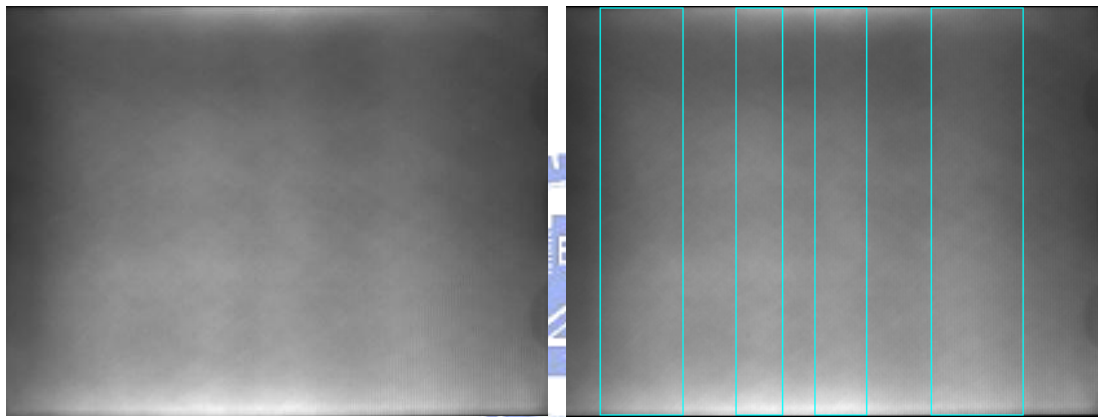
LCD panel NO.7

LCD panel NO.8

Figure 4-3 Vband detection result; threshold = 0.015, std of LOG = 5

Left: original images;

Right: detection results

Conclusions

In this paper an automatic Mura defection system is proposed. This system can detect four types of Mura defects.

1. To detect cluster Muras, the Laplacian of Gaussian (LOG) filter is used. The Cluster Mura is detected by multi-resolution LOG filters. A multi-resolution approach is proposed to detect cluster Muras of different scales.

2. To detect light leak Mura, we apply image mirroring and adopt the same LOG filter that has been used in detecting cluster Muras.

3. To detect v-band Mura, we check the variation tendency of the projected 1-D intensity profile. The curve fitting method is used and the sample points are the zero crossing points detected by a 1-D LOG filter.

4. To detect rubbing Mura, we designed a frequency mask to detect distinct components in the frequency domain. The summation power of distinct components within the masked frequency domain is then calculated to determine whether a rubbing Mura exists.

All four types of Mura detection algorithms have been integrated together in an efficient way. Simulation results have demonstrated that the proposed Mura detection algorithms are very reliable in automatically detecting Mura defects.

Bibliography

[1] Video Electronics Standards Association (VESA): Flat Panel Display Measurements Standard, version 2.0, p.78.

[2] Semiconductor Equipment and Materials International (SEMI) standard, "New Standard: Definition of Measurement Index (SEMU) for Luminance Mura in FPD Image Quality Inspection," draft number: 3324, pp. 1-6, 2002.

[3] Y. Mori, K. Tanahashi, and S. Tsuji, "Quantitative Evaluation of Visual Performance of Liquid Crystal Displays," Proceedings of the Algorithms and Systems for Optical Information Processing (The International Society for Optical Engineering), vol. 4113, pp. 242-249, 2000.

[4] Y. Mori, R. Yoshitake, T. TaMura, T. Yoshizawa and S. Tsuji, "Evaluation and Discrimination Method of "Mura" in Liquid Crystal Displays by Just Noticeable Difference Observation," SPIE (The International Society for Optical Engineering) Proceedings, vol. 4902, pp. 715-722, 2002.

[5] W. K. Pratt, S. S. Sawkar, and K. O'Reilly, "Automatic Blemish Detection in Liquid Crystal Flat Panel Displays," SPIE (The International Society for Optical Engineering) Proceedings, vol. 3306, pp. 2-13, 1998.

[6] V. Gibour and T. Leroux, "Automated, Eye-like Analysis of Mura Defects,"

Proceedings of SID (The Society for Information Displays), pp. 1440-1443, 2003.

[7]   Intel corp. patent, "Anti-Aliasing Diffractive Aperture and Optical System using the same," US. Patent: 5940217, Aug. 1999.

[8]   T. TaMura, M. Baba and T. Furuhata, "Effect of the Background Luminance on Just Noticeable Difference Contrast of 'Mura' in LCDs," Proceedings of SID (The International Society for Optical Engineering), pp. 1527-1530, 2003.

[9]   D. G. Lee, I. H. Kim, M. C. Jeong, B. K. Oh, and W. Y. Kim, "Mura Analysis Method by Using JND Luminance And the SEMU Definition," Proceedings of SID (The International Society for Optical Engineering), pp. 1467-1470, 2003.

[10] Jong-Hwan Oh, Dong-Ming, Kyu-Bong Lee, Young-Chul Song, Doo-Hyun Choi and Kil-Houm Park, "Line Defect Detection in Tft-Lcd Using Directional Filter Bank and Adaptive Multilevel Thresholding", Trans Tech Publications, Switzerlang Vols. 270-273 (2004) pp. 233-238

[11] Woo-Seob Kim, Dong-Min Kwak, Young-Chul Song, Doo-Hyun Choi and Kil-Houm Park, "Detection of Spot-Type Defects on Liquid Crystal Display Modules" Trans Tech Publications, Switzerlang Vols. 270-273 (2004) pp. 808-813

[12] Jae Y. LEE and Suk I.YOO, "Automatic Detection of Region-Mura Detect in TFT-LCD", IECIE transaction inf. & syst. Vol. E87-D, No. 10, October 2004.

[13] Hsin-Chia Chen, Li-Te Fang, Sheng-Jyh Wang, "LOG Filter Based Inspection of

Cluster Mura and Vertical Band Mura on Liquid Crystal Displays", SPIE transaction [EI 5679-30], January, 2005.

[14] E. Peli, "Contrast in complex images", J. Opt. Soc. Amer. A, vol. 7, pp. 2032-2039, October 1990.

[15] E. Peli, "In search of a contrast metric: Matching the perceived contrast of Gabor patches at different phases and bandwidths," Vision *Re*s. 37(23), pp. 3217-3224, 1997.

[16] J. L. Mannos and D. J. Sakrison, "The effect of a visual fidelity criterion on the encoding of images", *IEEE Trans. Inform. Theory,* vol. IT-20, pp. 525-536, July 1974.
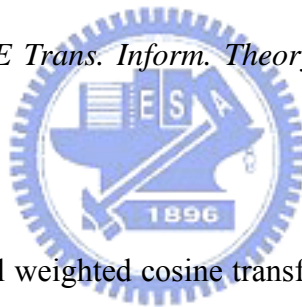
[17] N. B. Nill, "A visual model weighted cosine transform for image compression and quality assessment", *IEEE Trans. Commun.,* vol. COM-33, pp. 551-557, June 1985.

[18] K. N. Ngan, K. S. Leong, and H. Singh, "Cosine transform coding incorporating human visual system model", presented at SPIE Fiber '86, Cambridge, MA, pp. 165-171, September 1986.

[19] D. H. Kelly, "Motion and vision II. stabilized spatial-temporal surface", *J. Opts. Soc. Amer.*, vol. 69, pp. 1340-1349, October 1979.

[20] I. Vujovic, I. Kuzmanic, and M. Krcum, "Experimental Results in Visibility

Threshold in Human Visual Perception for Application in Image/Video Coding Quality Assessment", IEEE Region 8 International Symposium on Video/Image Processing and Multimedia Communications 16-19, June 2002.

[21] C. –H. Chou and C. –W. Chen, "A Perceptually Optimized 3-D Subband Codec for Video Communication over Wireless Channels", *IEEE transactions on circuits and systems for video technology,* vol.6, no.2, April, 1996.

[22] C. –H. Chou and Y. –C. Li, "A Perceptually Tuned Subband Image Coder Based on the Measure of Just-Noticeable-Distortion Profile", *IEEE Transactions on Circuits and Systems for Video Technology,* vol.5, no.6, December 1995